Towards the study of the Solar wind Effects on the Magnetosphere using Fully Kinetic Simulations

Jorge AMAYA[1], Jan DECA[1], Stefano Markidis[2], Andrei DIVIN[3], Bertrand Lembège[4], Giovanni LAPENTA[1]

[1]CPA, KULeuven, Belgium
[2]KTH Royal Institute of Technology, Sweden
[3]Institutet för rymdfysik, Uppsala Universitet, Sweden
[4]LATMOS, CNRS, France

KU LEUVEN

EU FP7 projects

- SWIFF: Space Weather Integrated Forecasting Framework (n° 263340)
- eHeroes: Environment for Human Exploration and RObotic Experimentation in Space (n° 284461)
- DEEP: Dynamical Exascale Entry Platform (n° 287530)

SEVENTH FRAMEWORK PROGRAMME

Motivation: Space Weather

- Complex plasma physics
- From fluid to kinetic effects
- From electron to planetary scales
- Highly coupled phenomena
- Effects on human and robotic space exploration

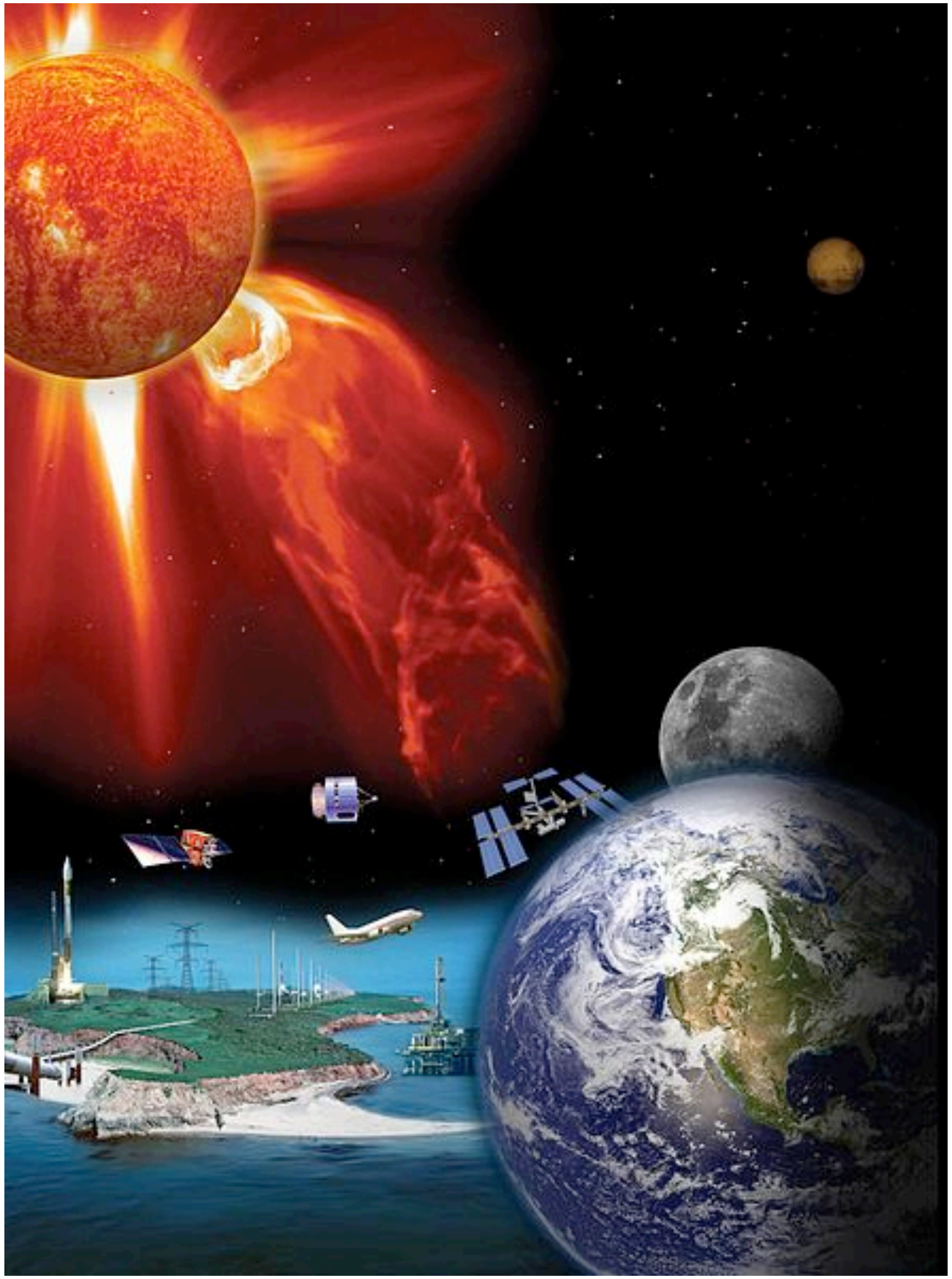

Different time and space scales

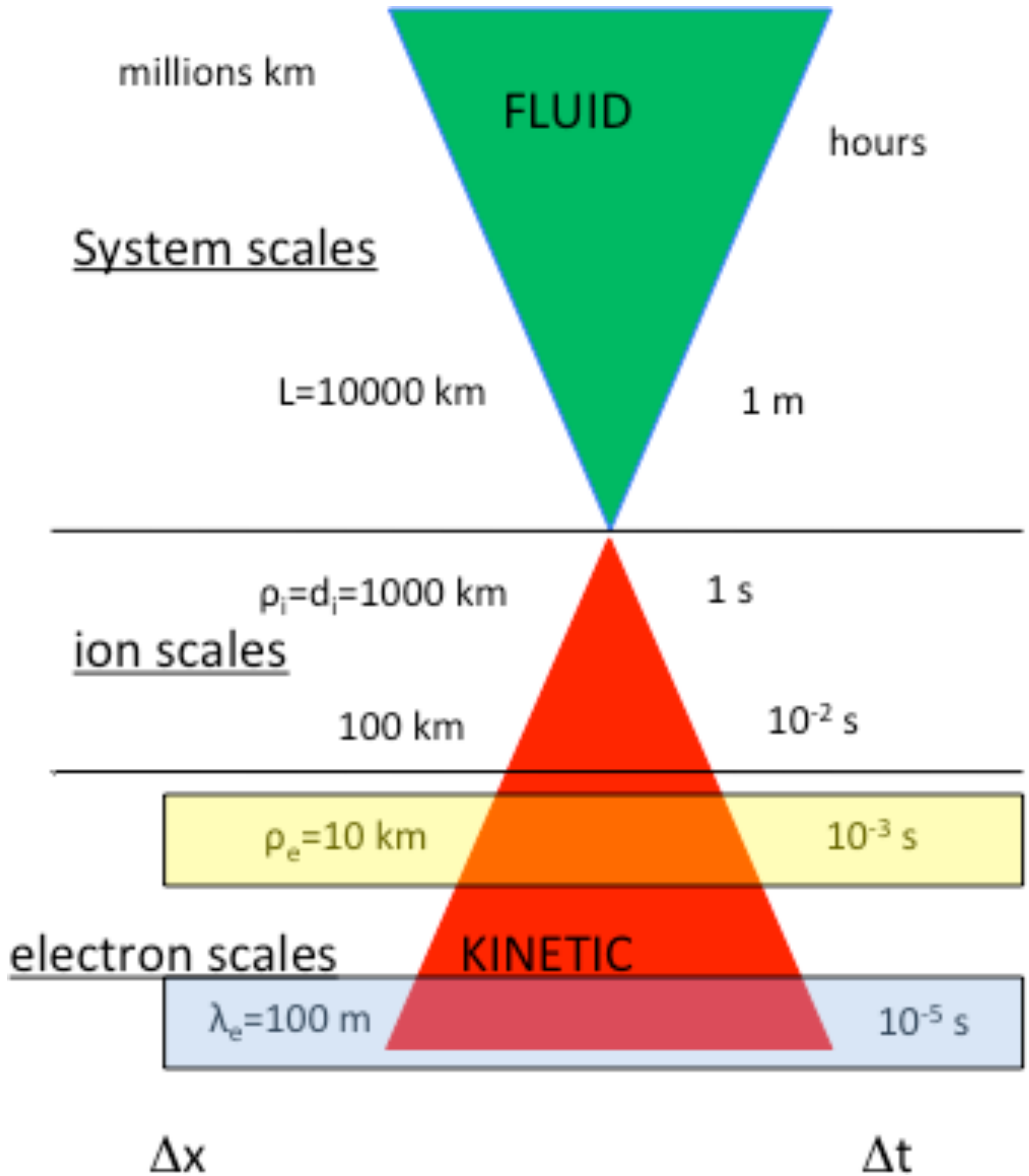

Numerical methods

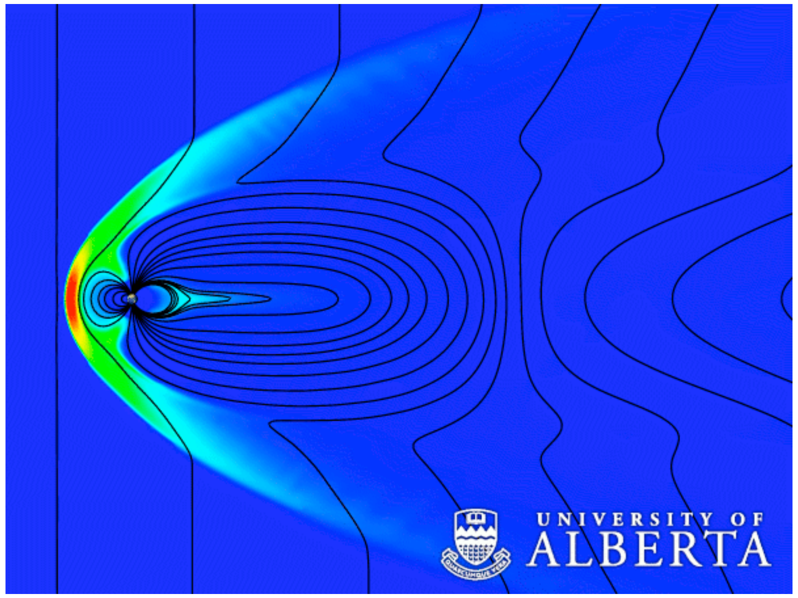

N. Omidi et al. / Advances in Space Research 38 (2006) 632–638

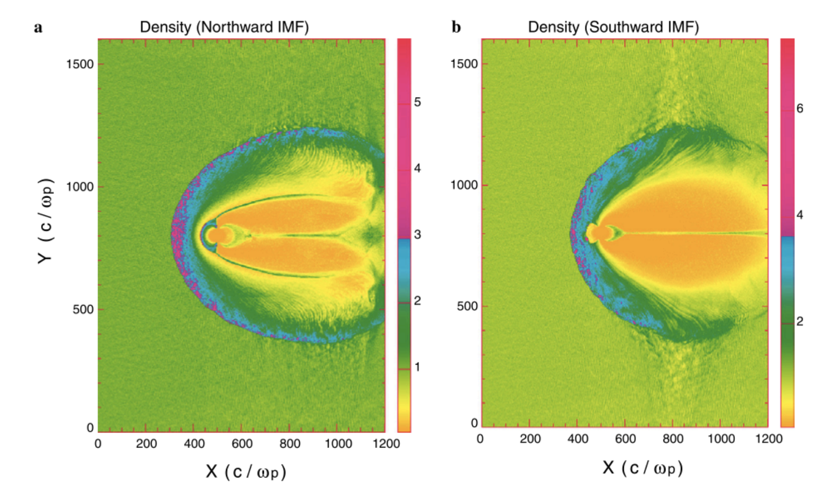

Fig. 1. Density (normalized to solar wind density) as a function of X and Y during (a) northward and (b) southward IMF.

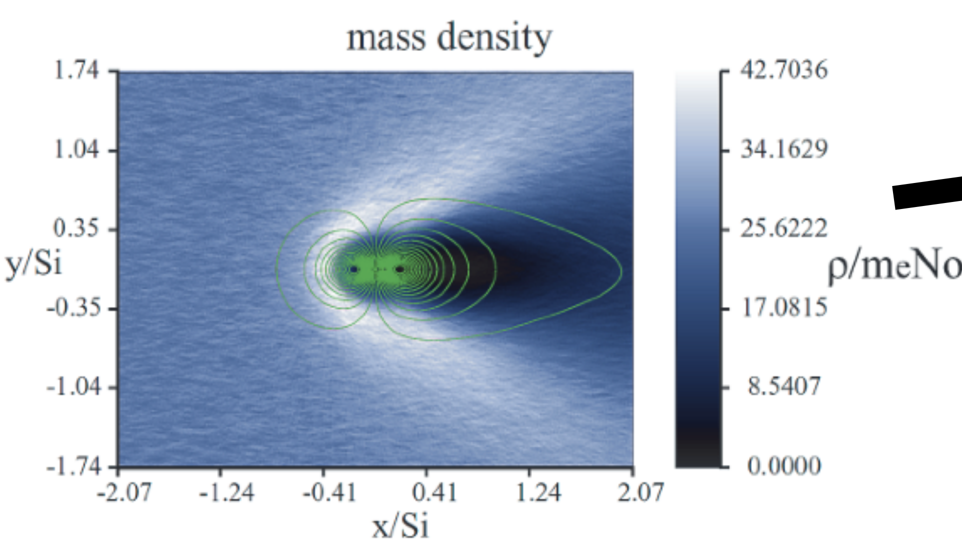

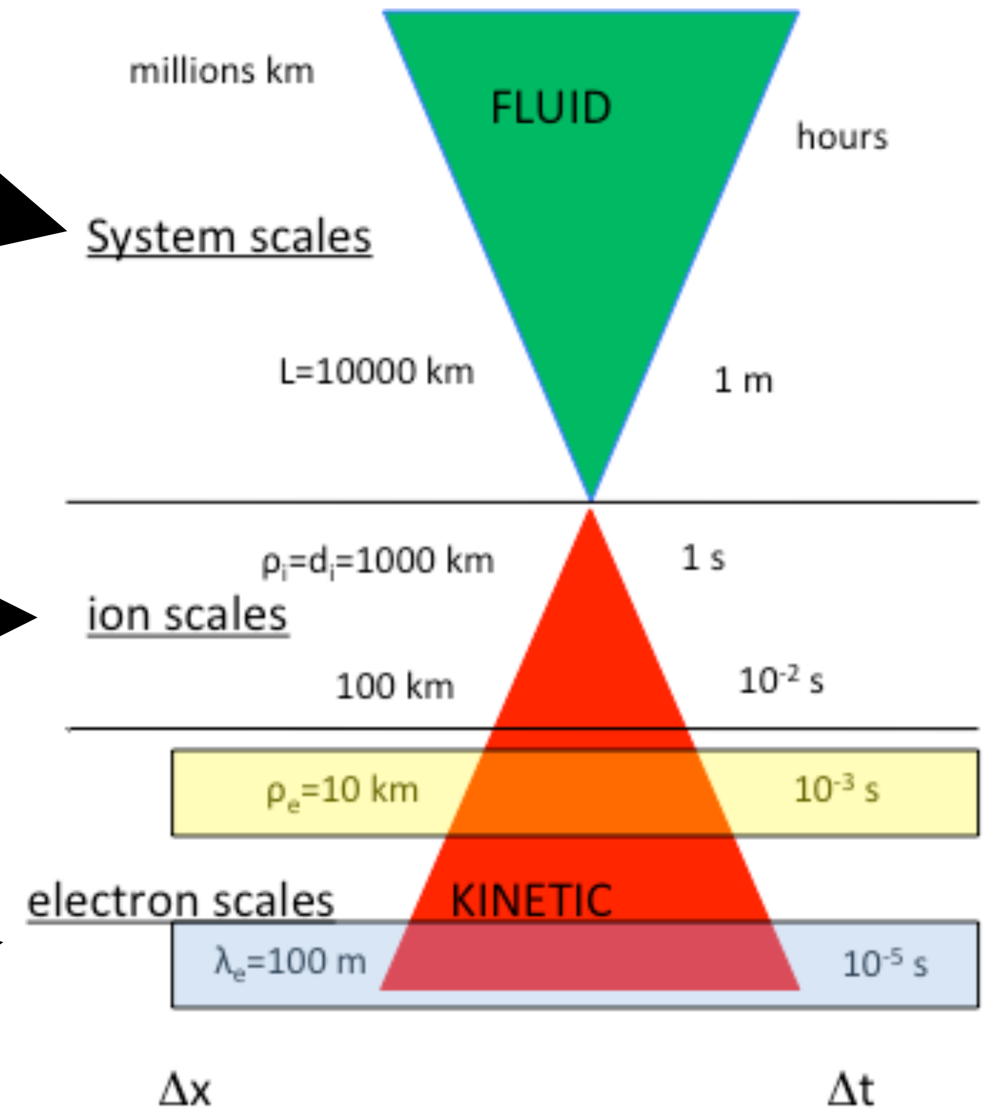

[1] University of Alberta web page.
[2] N. Omidi et al., Advances in Space Research, Volume 38, Issue 4, 2006
[3] Toseo Moritaka, et al., Phys. Plasmas 19, 032111, 2012

Fully kinetic

[1] S. Baraka and L. Ben-Jaffel, Ann. Geophys., 29, 2011

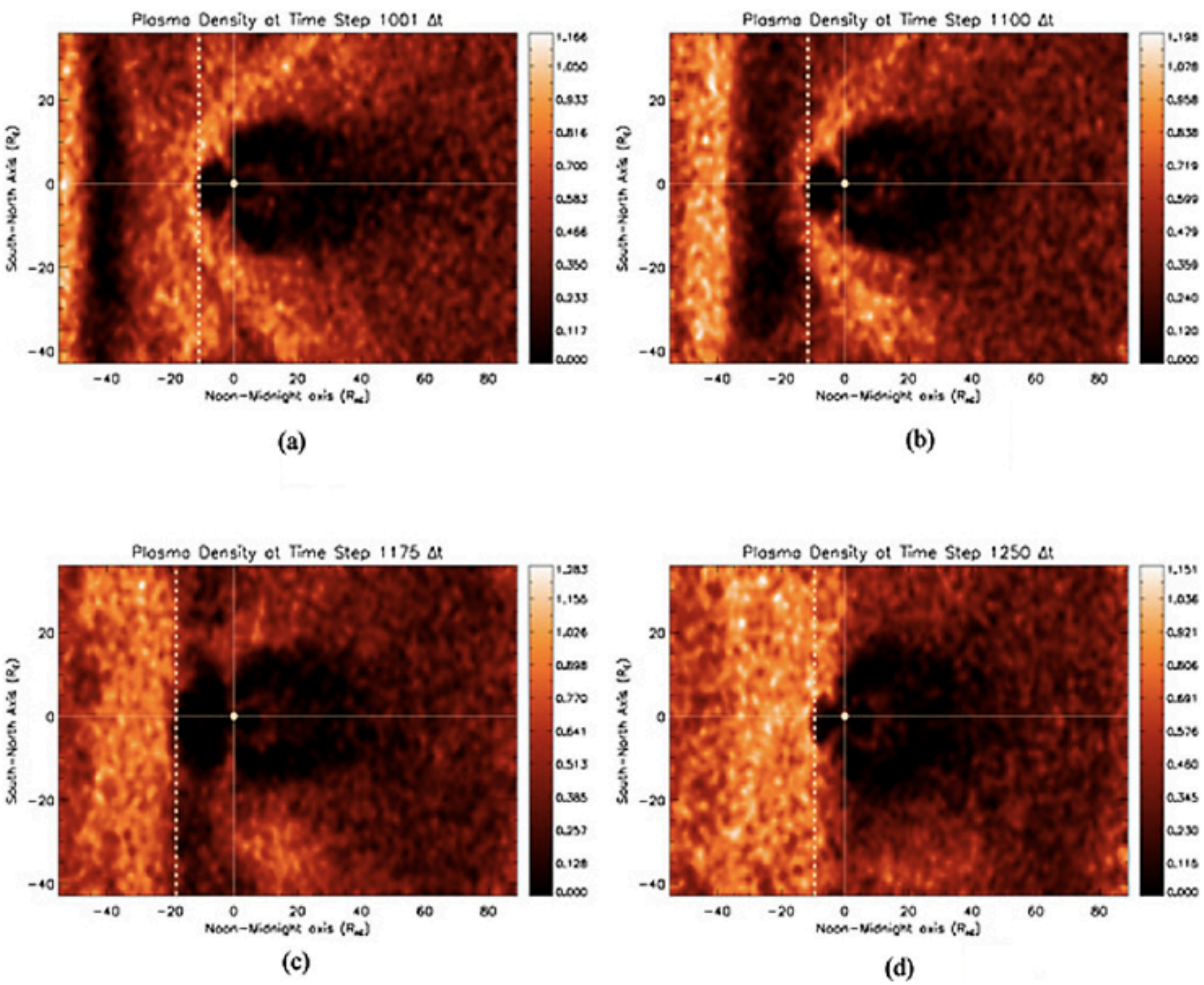

Density

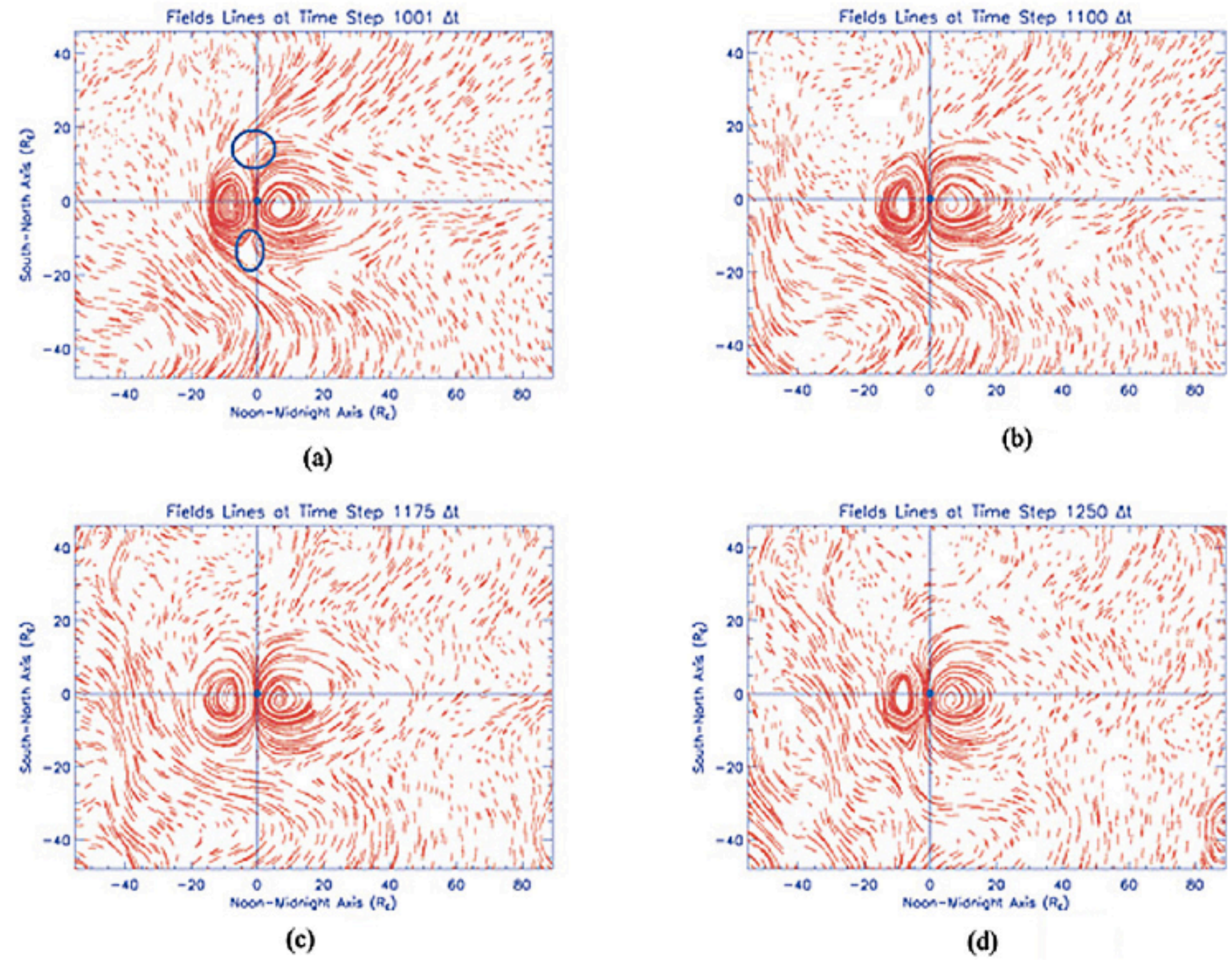

Magnetic field

$$\Delta x = 1R_E, \;\; V_{sw}/c = 0.5, \;\; \Delta t = 3.6sec.$$

$$m_i/m_e = 16, \;\; v_{th,e}/c = 0.1, \;\; v_{th,i}/c = 0.025$$

PiC simulations at ion-scales

[1] M. Matsumoto et al., Plasma and Fusion Research, 8, 2013

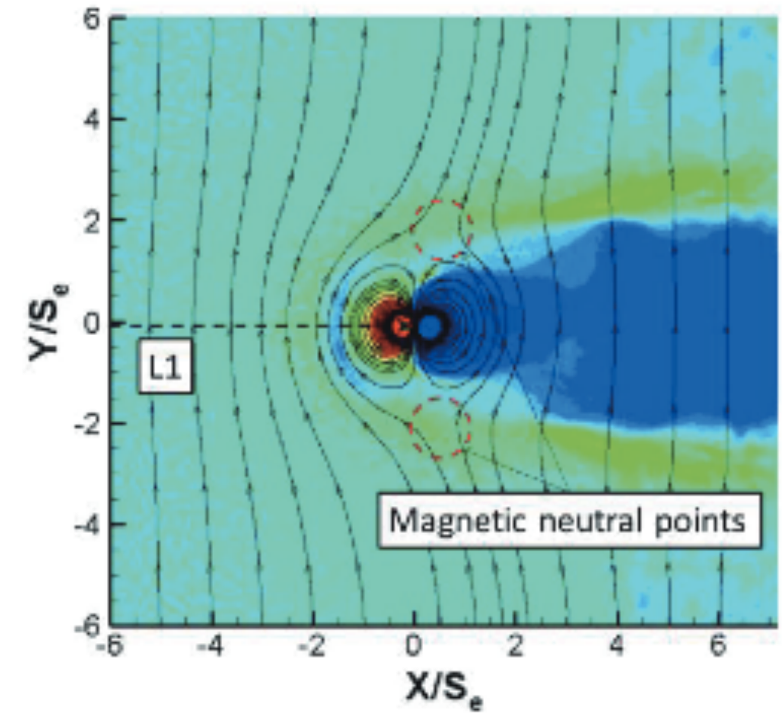

(a) Case with +Y direction IMF

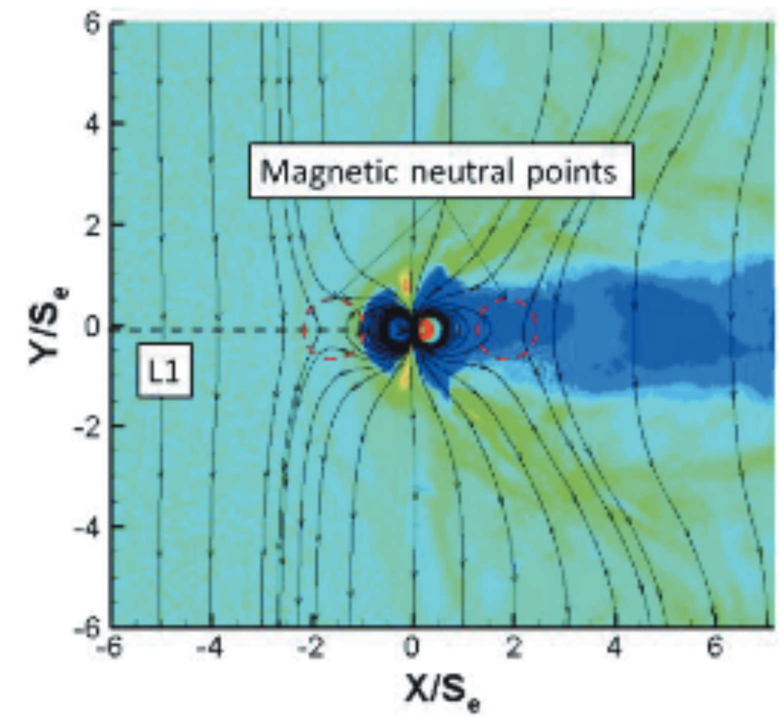

(b) Case with −Y direction IMF

- Adaptative mesh refinemet.
- Ion-scale simulation: applications to spacecraft shielding and magnetic sails

Global 3D PiC

[1] Cai et al., Earth Planets Space, 53, 2001

Global magnetospheric 3D topology

$$215 \times 95 \times 95$$
$$m_i/m_e = 16$$
$$v_{sw}/c = 0.5$$
$$v_{th,e}/c = 0.2$$
$$v_{th,i}/c = 0.05$$

D. CAI *et al.*: THREE-DIMENSIONAL MAGNETIC FIELD TOPOLOGY

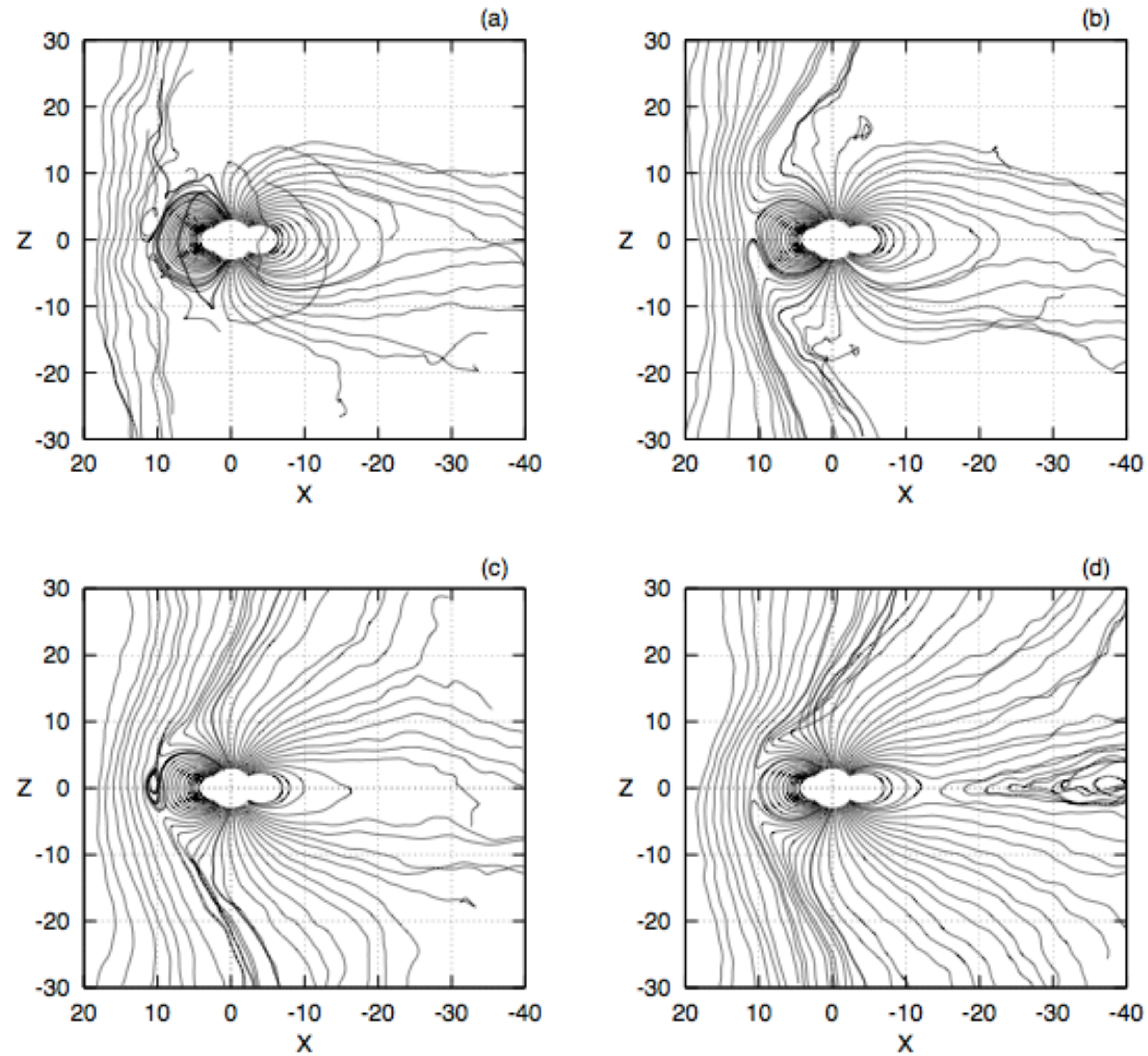

Hybrid codes: Mercury magnetosphere

$$1200 \times 1600$$
$$\beta = 0.5$$
$$\Delta x = 1 d_i$$
$$R = 30 d_i$$
$$M = 2$$

N. Omidi et al. / Advances in Space Research 38 (2006) 632–638

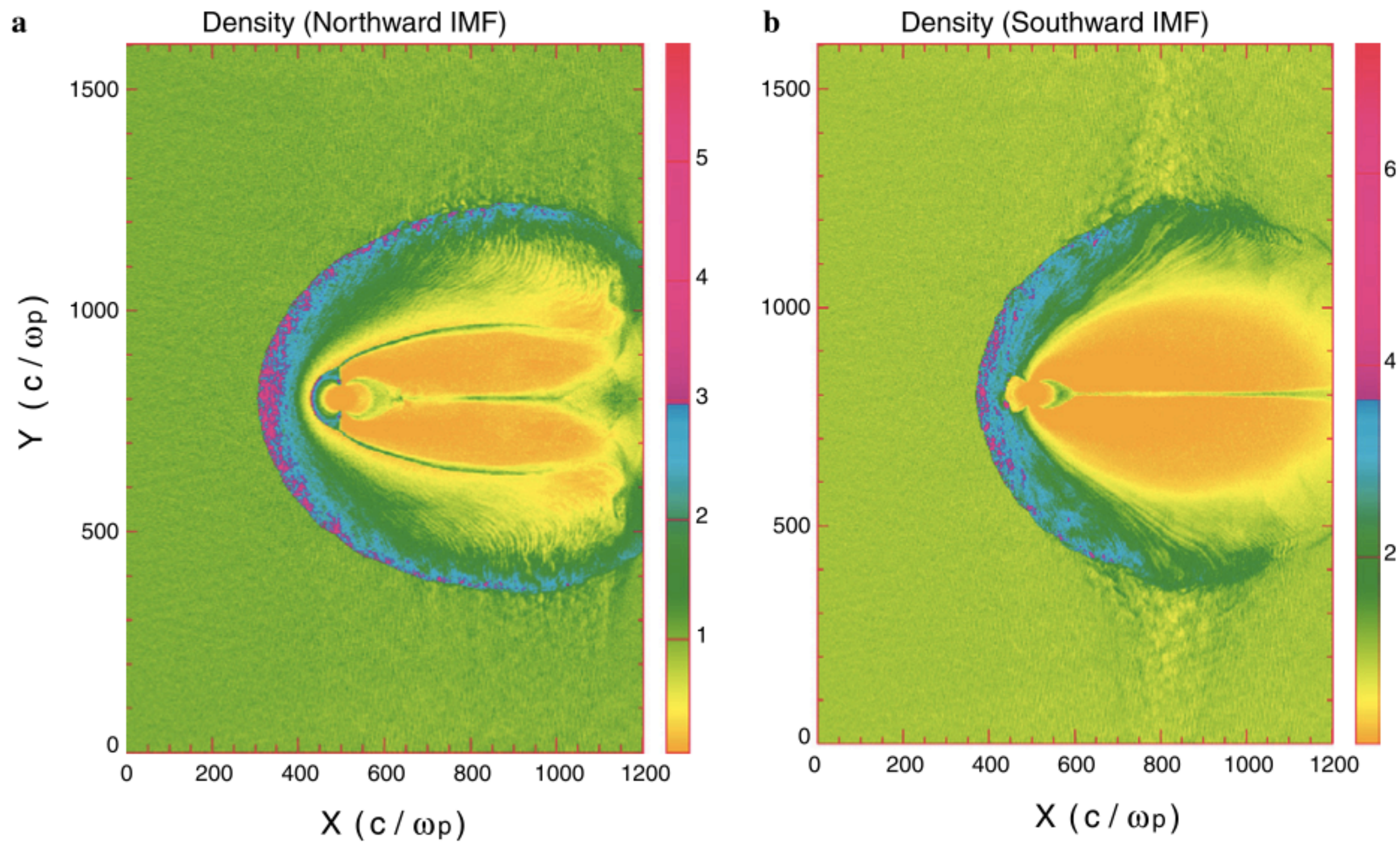

Fig. 1. Density (normalized to solar wind density) as a function of X and Y during (a) northward and (b) southward IMF.

Hybrid-Vlasov codes

- Solving above ion scales.
- Capture of wave propagation in the foreshock and the magnetosheat.
- Resolution in spatial (2D) and velocity (3D) spaces.

$$\Delta x = 0.13 R_E$$
$$\Delta v = 20 km/s$$

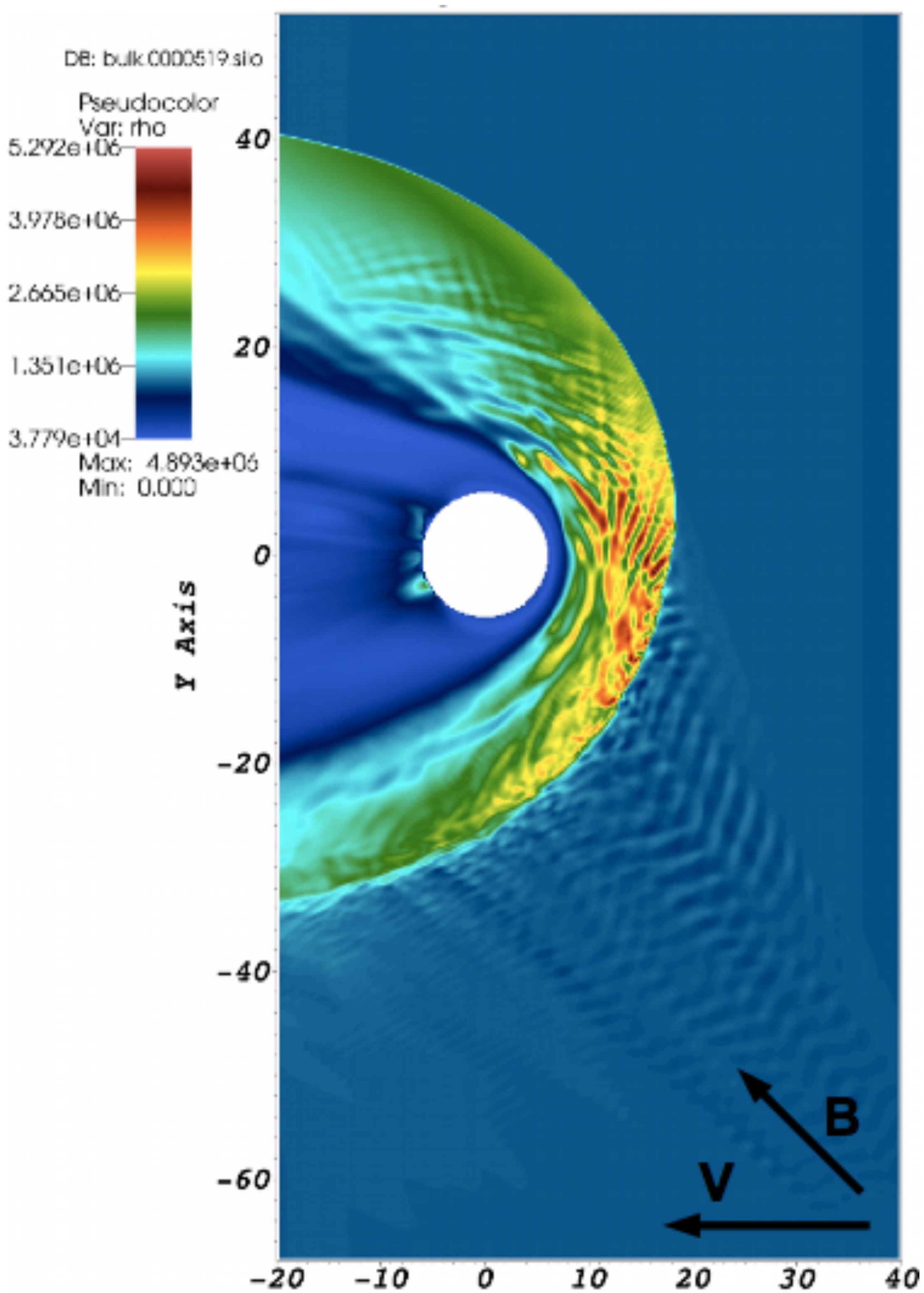

Tha Particle-in-Cell method

PARTICLES

$$\frac{d\vec{\mathbf{x}}_p}{dt} = \vec{\mathbf{v}}_p$$

$$m_s \frac{d\vec{\mathbf{v}}_p}{dt} = q_s(\vec{\mathbf{E}}_p + \vec{\mathbf{v}}_p \times \vec{\mathbf{B}}_p)$$

$$\rho, \vec{\mathbf{J}} \longrightarrow$$

Interpolation

$$\longleftarrow \vec{\mathbf{E}}_p, \vec{\mathbf{B}}_p$$

FIELDS

$$\nabla \cdot \vec{\mathbf{E}} = \rho/\epsilon_0$$

$$\nabla \cdot \vec{\mathbf{B}} = 0$$

$$\nabla \times \vec{\mathbf{E}} + \frac{\partial \vec{\mathbf{B}}}{\partial t} = 0$$

$$\nabla \times \vec{\mathbf{B}} - \epsilon_0 \mu_0 \frac{\partial \vec{\mathbf{E}}}{\partial t} = \mu_0 \vec{\mathbf{J}}$$

Implicit equations

Particles:

$$\mathbf{x}_p^{n+1} = \mathbf{x}_p^n + \mathbf{v}_p^{n+1/2}\Delta t,$$

$$\mathbf{v}_p^{n+1} = \mathbf{v}_p^n + \frac{q_s \Delta t}{m_s}\left(\mathbf{E}_p^{n+\theta}(\mathbf{x}_p^{n+1/2}) + \mathbf{v}_p^{n+1/2} \times \mathbf{B}_p^n(\mathbf{x}_p^{n+1/2})\right)$$

Fields:

$$\mathbf{B}_g^{n+1} - \mathbf{B}_g^n = -\Delta t \nabla \times \mathbf{E}_g^{n+\theta},$$

$$\mathbf{E}_g^{n+1} - \mathbf{E}_g^n = \frac{\Delta t}{\mu_0 \epsilon_0}\left(\nabla \times \mathbf{B}_g^{n+\theta} - \mu_0 \mathbf{J}_g^{n+\frac{1}{2}}\right),$$

$$\epsilon_0 \nabla \cdot \mathbf{E}_g^{n+\theta} = \rho_g^{n+\theta},$$

$$\nabla \cdot \mathbf{B}_g^{n+1} = 0.$$

Stability condition: $v_{\mathrm{th},e}\Delta t/\Delta x < 1.$

Advantages of the iPic3D code

- Self-consistent.
- Implicit methods allow a wider range of time and space scales
- Highly scalable: improves with technology which makes it perfect for ExaScale systems
- Simple enough to port to new architectures

Disadvantages of the PiC method

- Particle noise: requires higher resolution.
- Boundary conditions: requires improved numerical methods.
- CPU cost: requires to work on new architectures and better algorithms.
- Problem size: coupled and multi-domain algorithms are being developed.

Current objectives

- Simulation parametters closer to the actual physics.
- 3 types of simulations:
  - A. 2D Noon-Midnight meridian plane
  - B. 2D Equatorial plane
  - C. 3D

A. Noon-midnight meridian plane

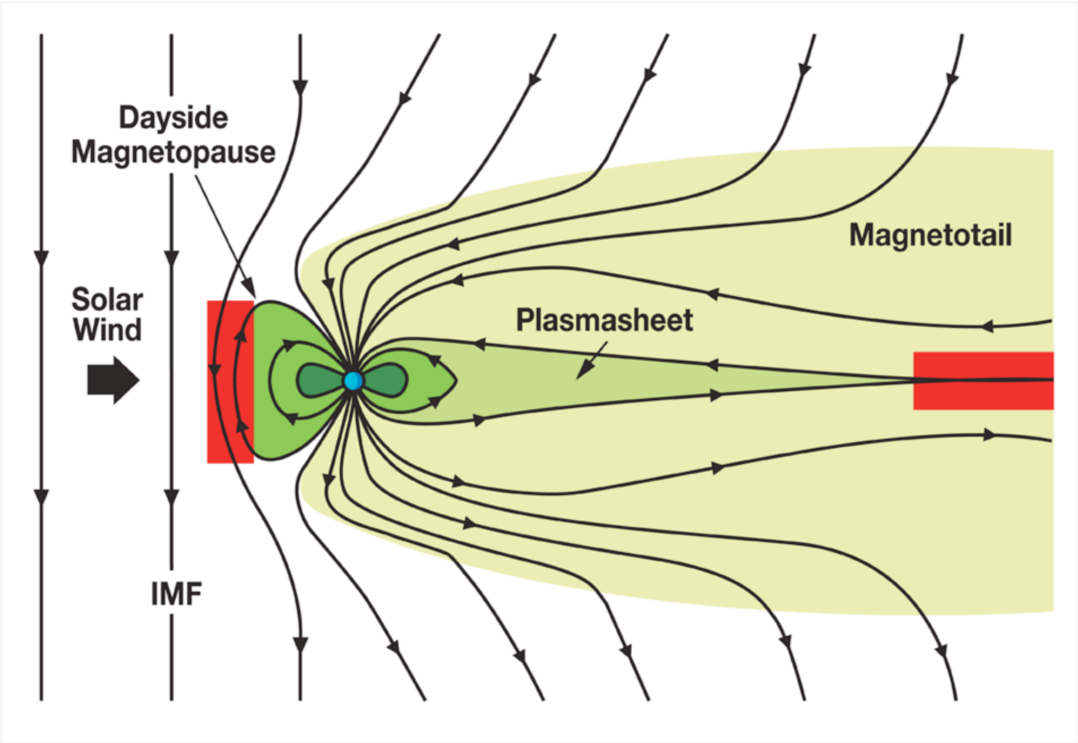

Reconnection

A. Noon-midnight meridian plane

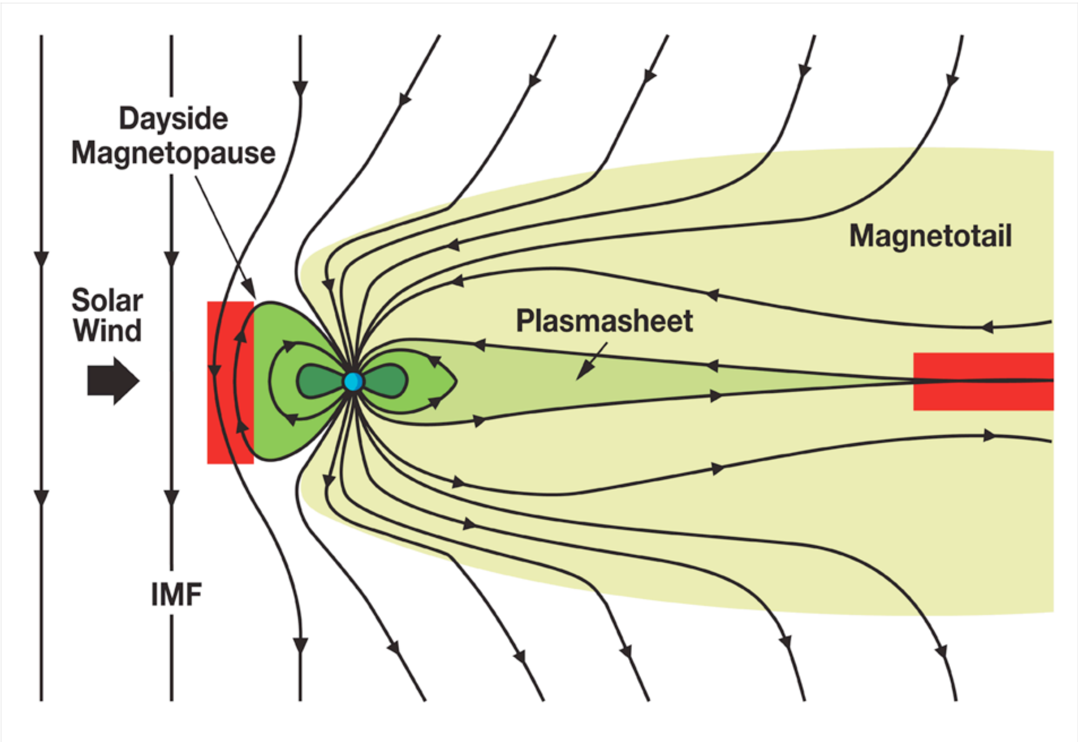

Reconnection

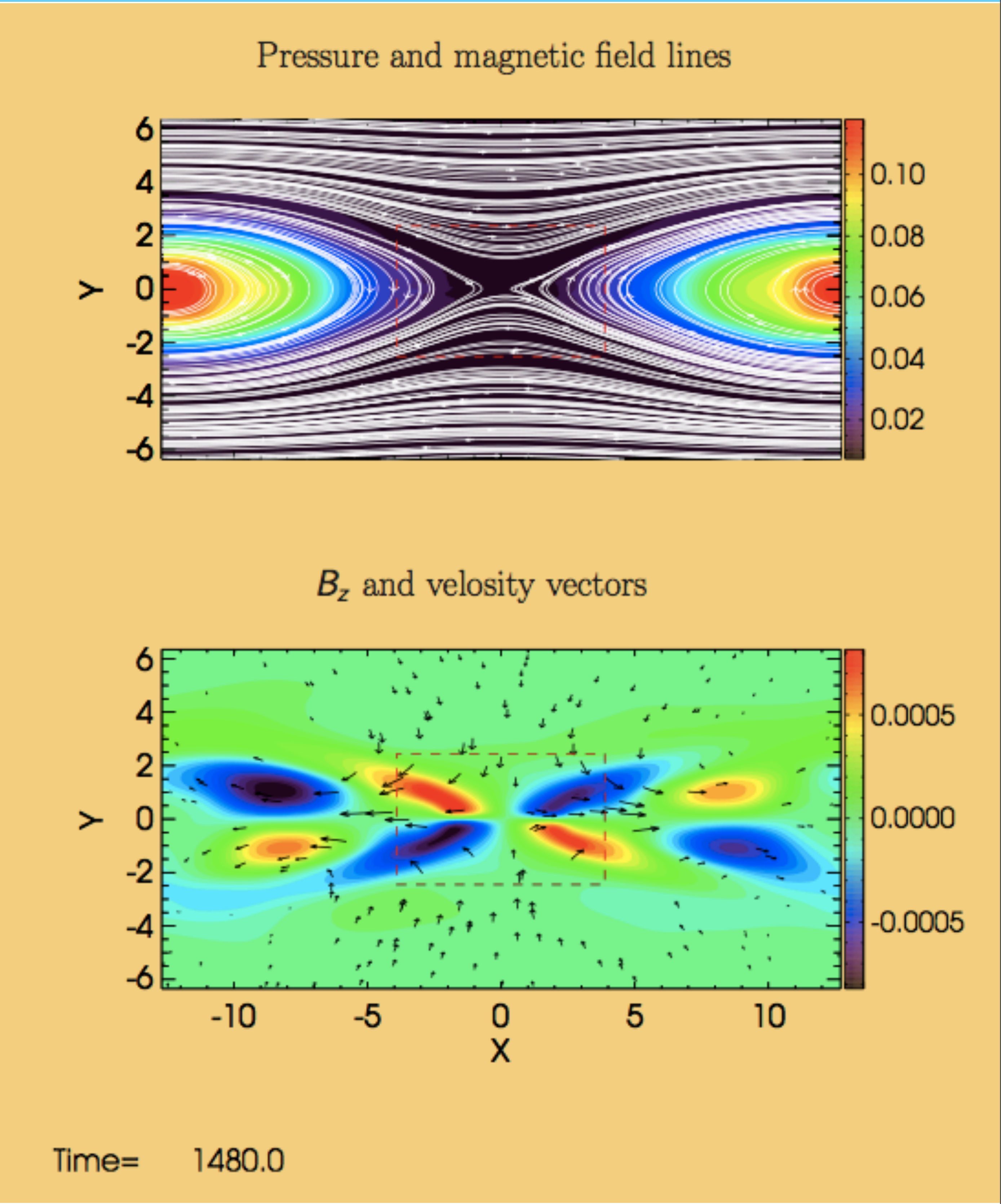

A. Noon-midnight meridian plane

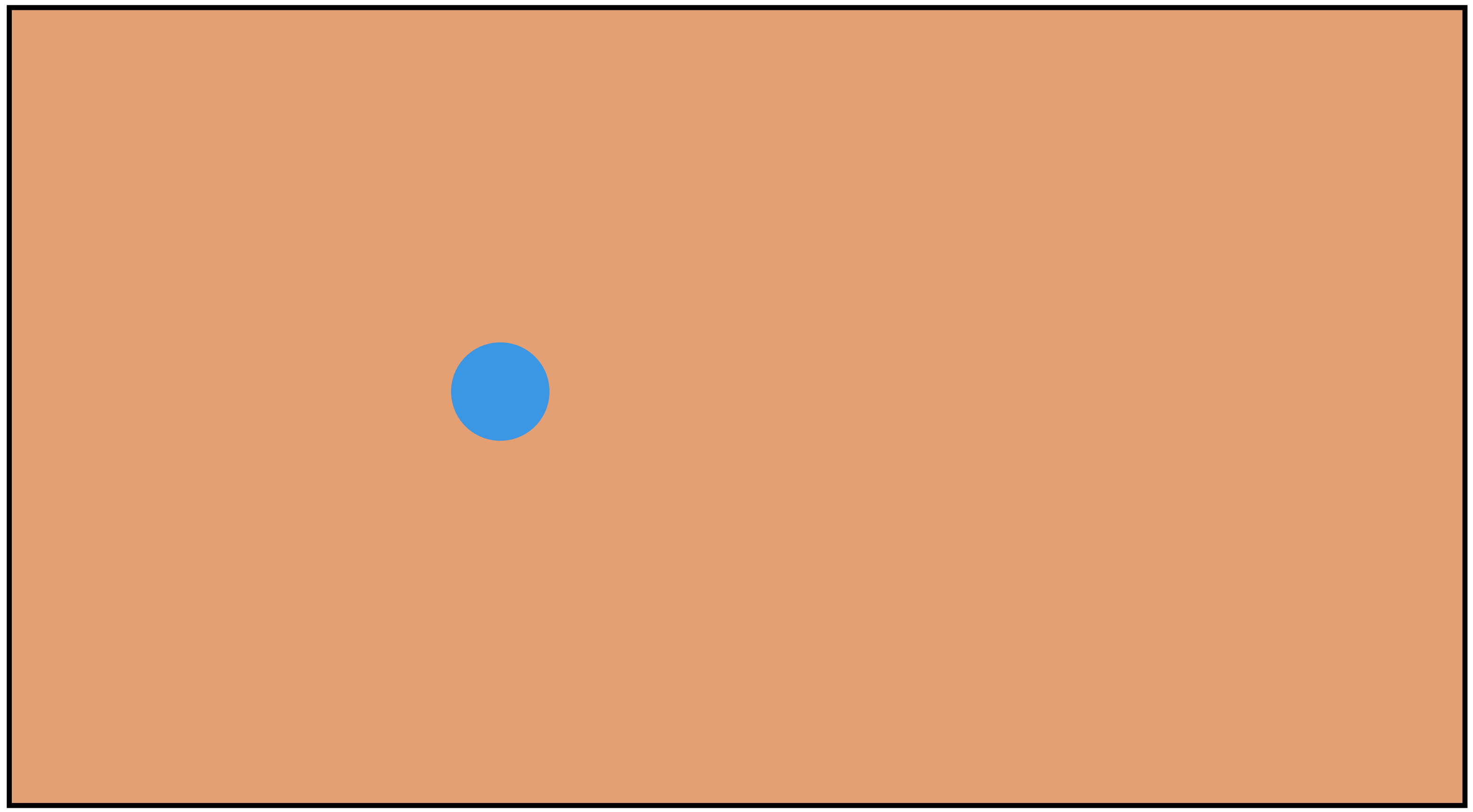

A. Noon-midnight meridian plane

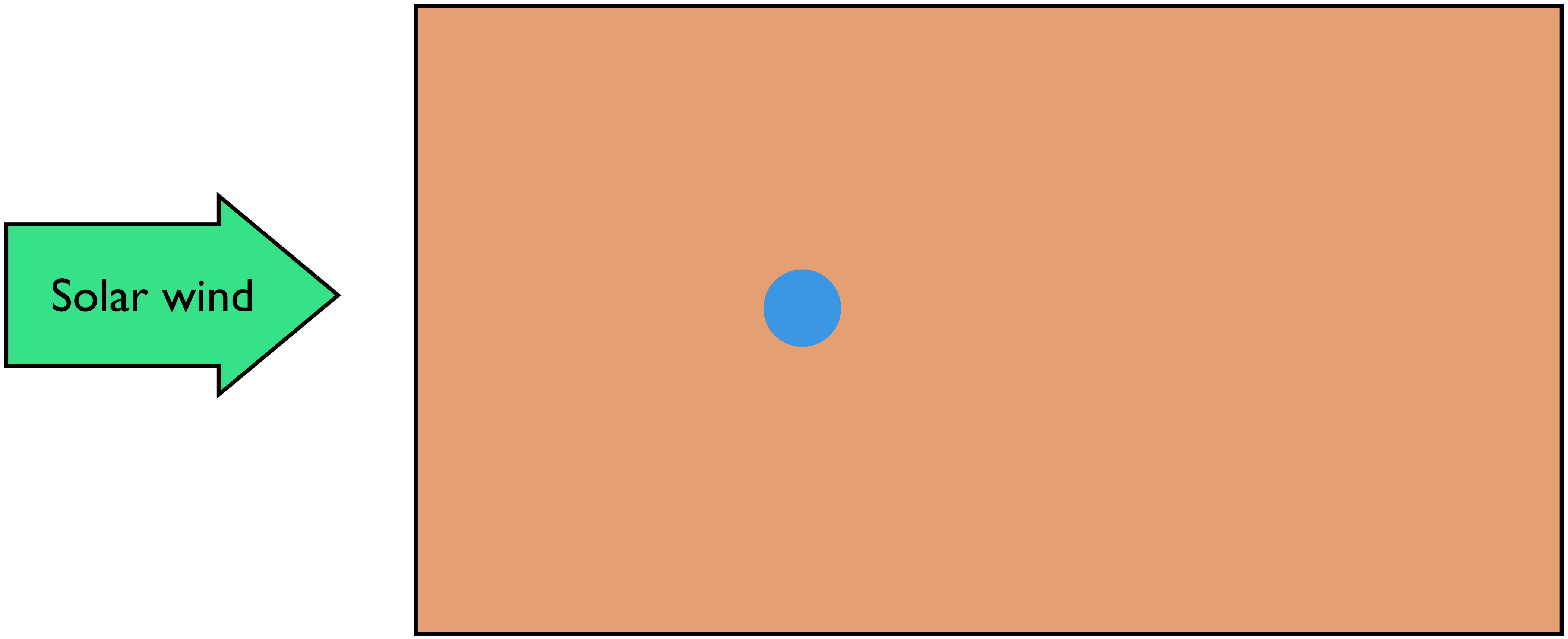

A. Noon-midnight meridian plane

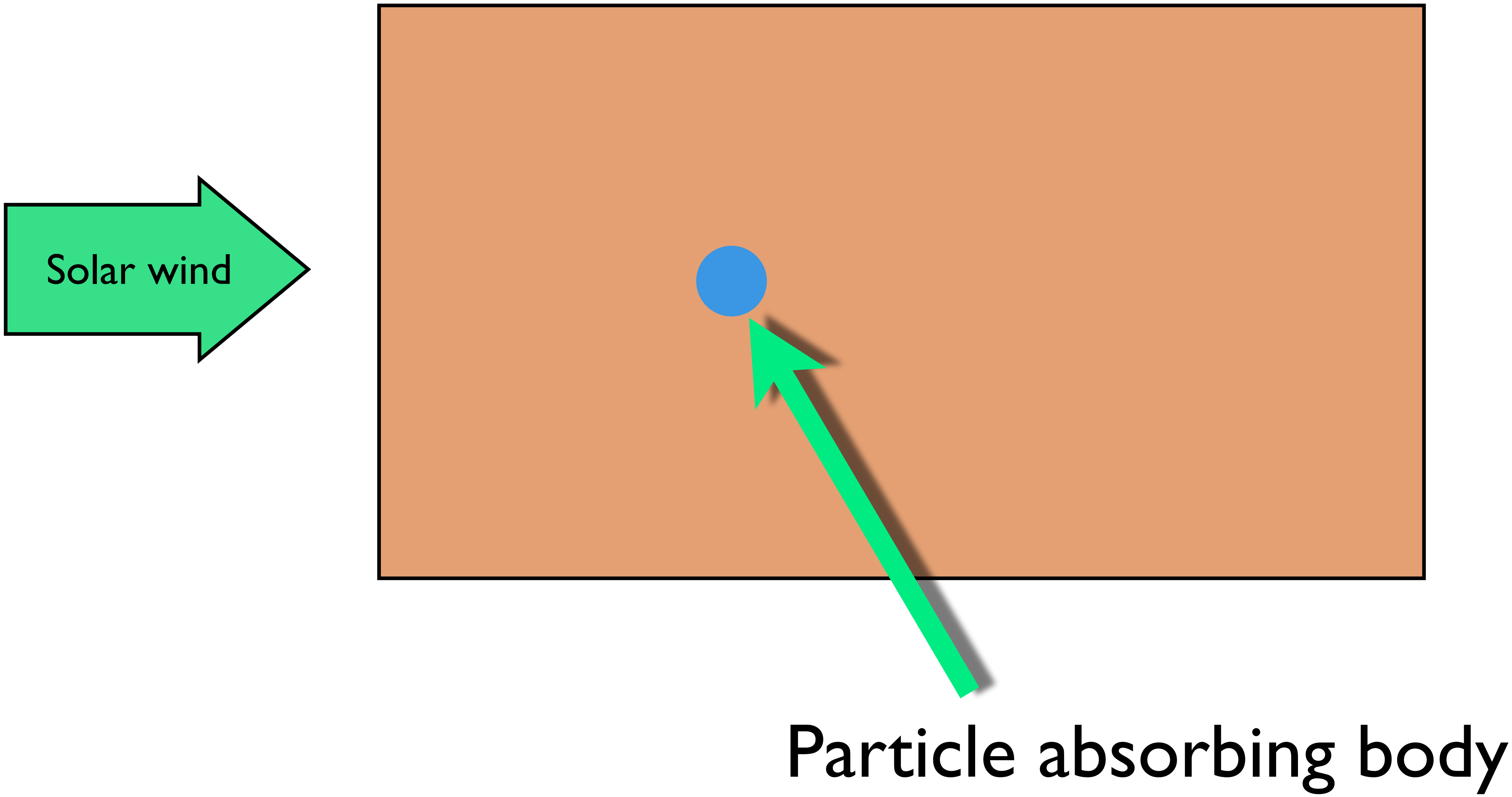

A. Noon-midnight meridian plane

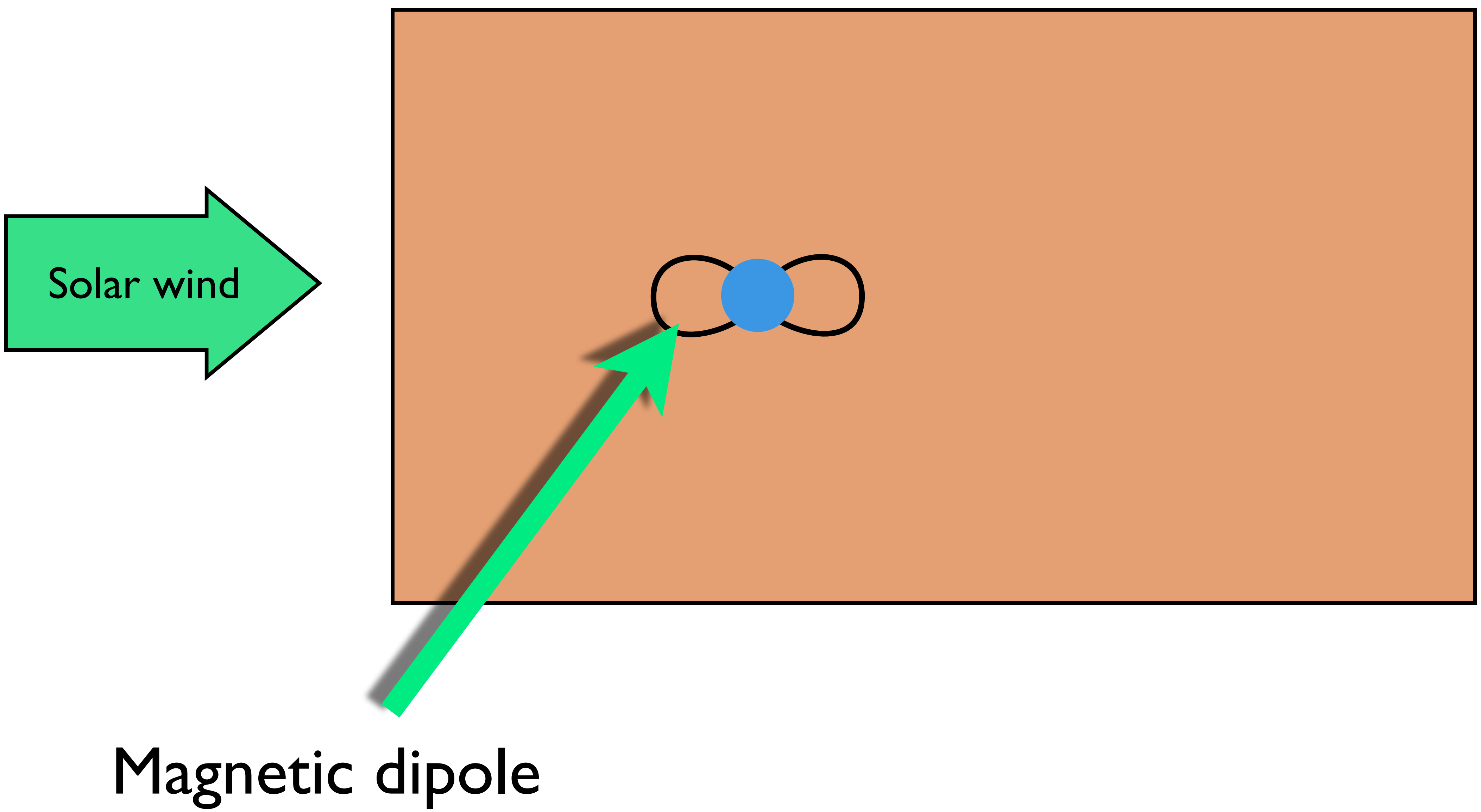

A. Noon-midnight meridian plane

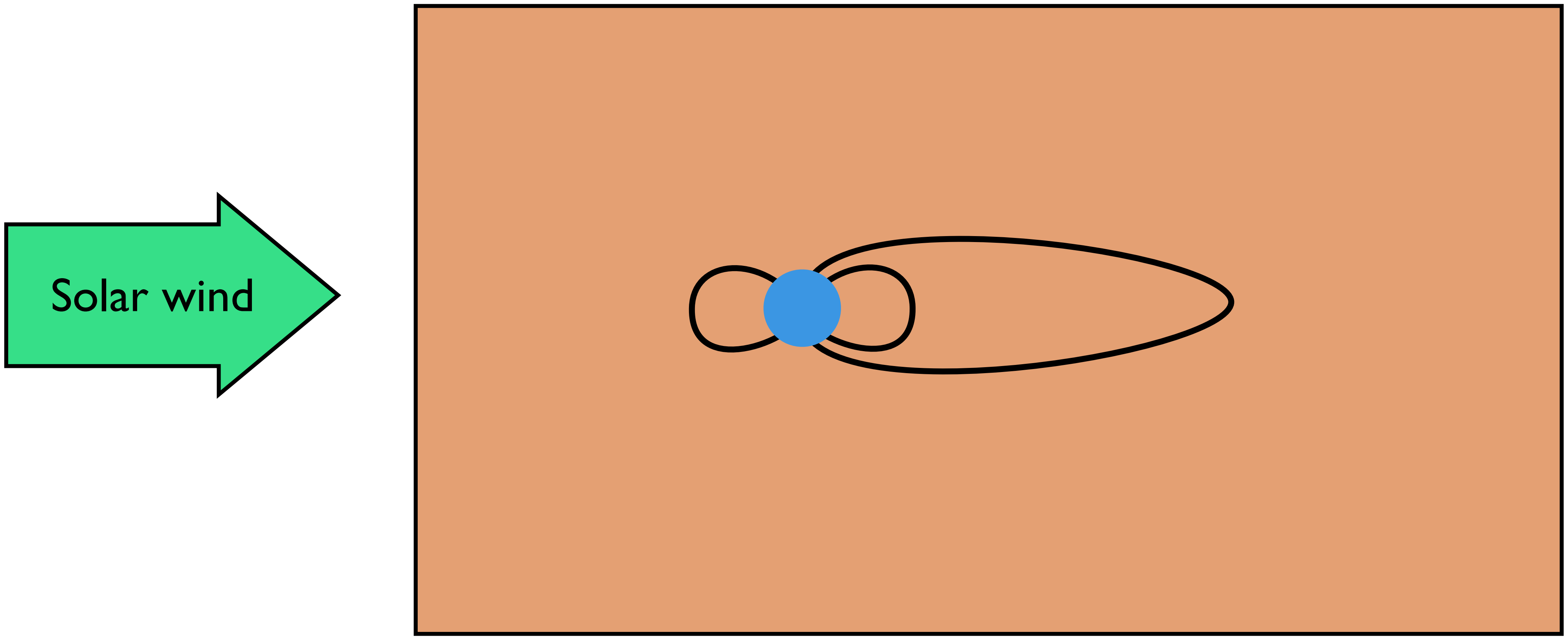

KU LEUVEN

A. Noon-midnight meridian plane

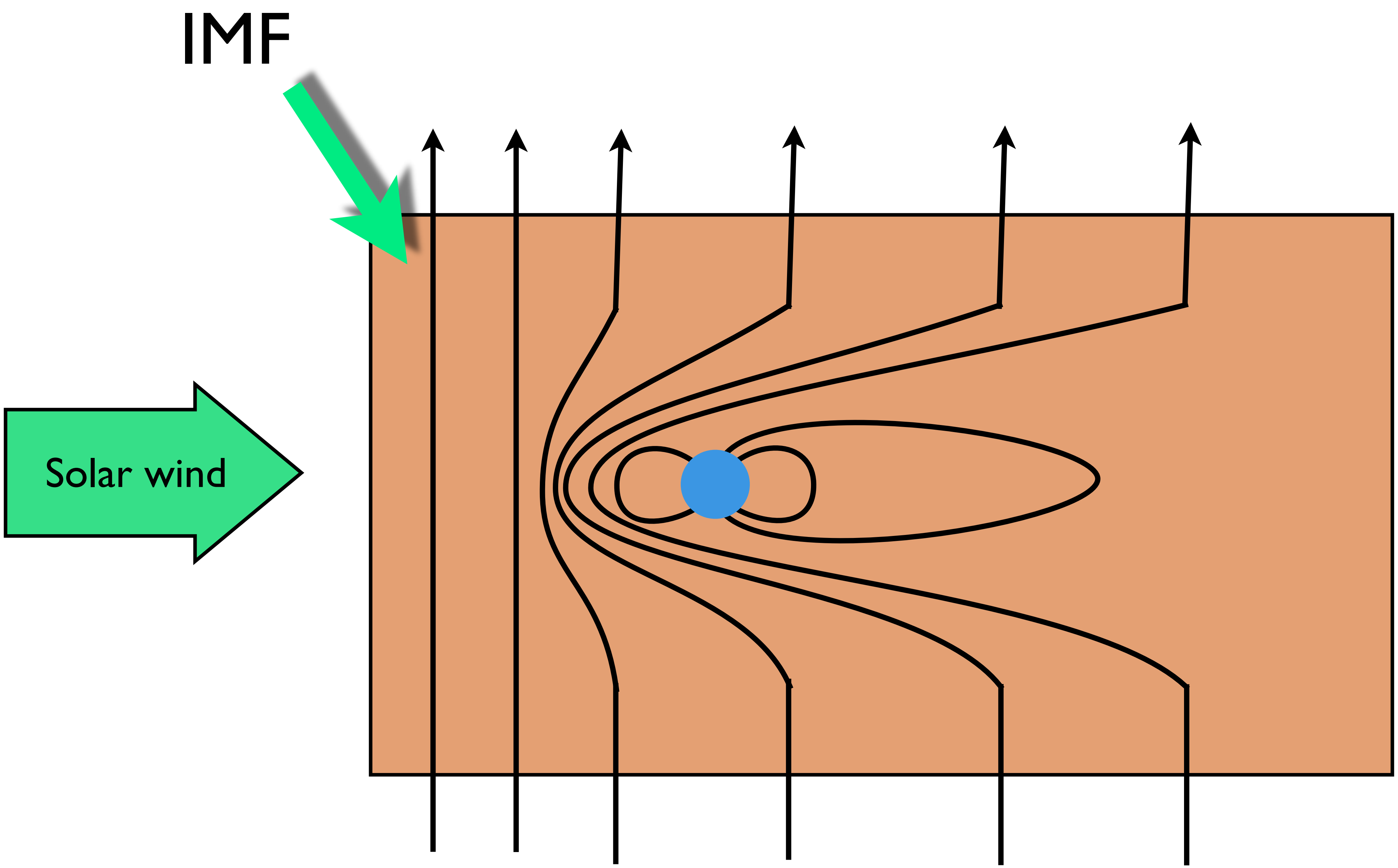

A. Noon-meridianidnight meridian plane

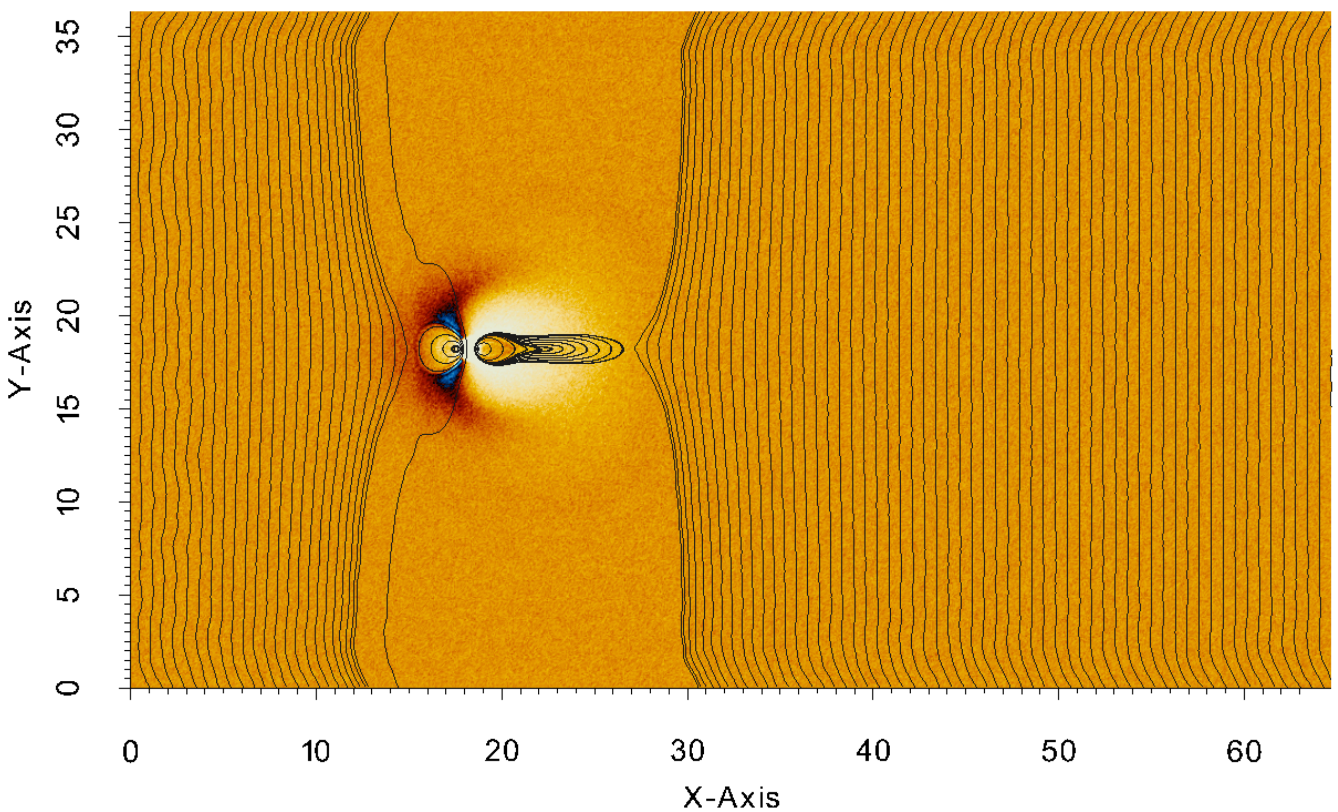

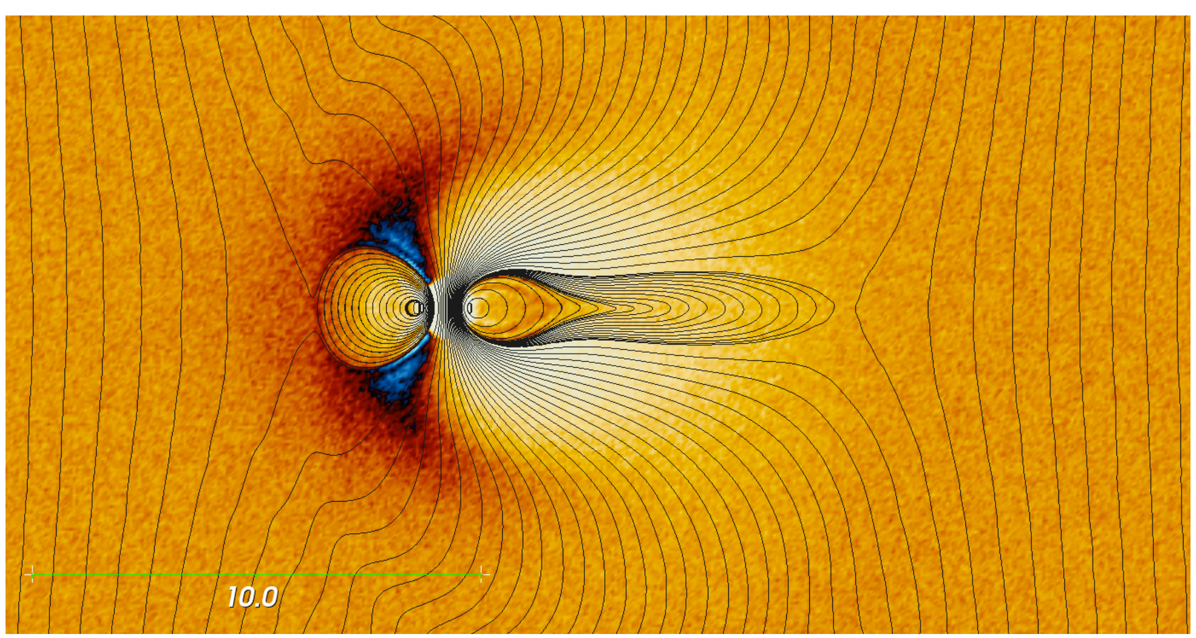

$$L_x = 64.768 d_i$$

$$L_y = 36.432 d_i$$

$$N = 1024 \times 576 = 589\,824$$

$$\Delta x = \Delta y = 0.06325 d_i$$

$$V_{sw}/c = 0.015$$

$$V_{th,e}/c = 0.05$$

$$V_{th,i}/c = 7.4 \times 10^{-3}$$

$$m_i/me = 250$$

$$M_A = 5$$

A. Noon-meridianidnight meridian plane

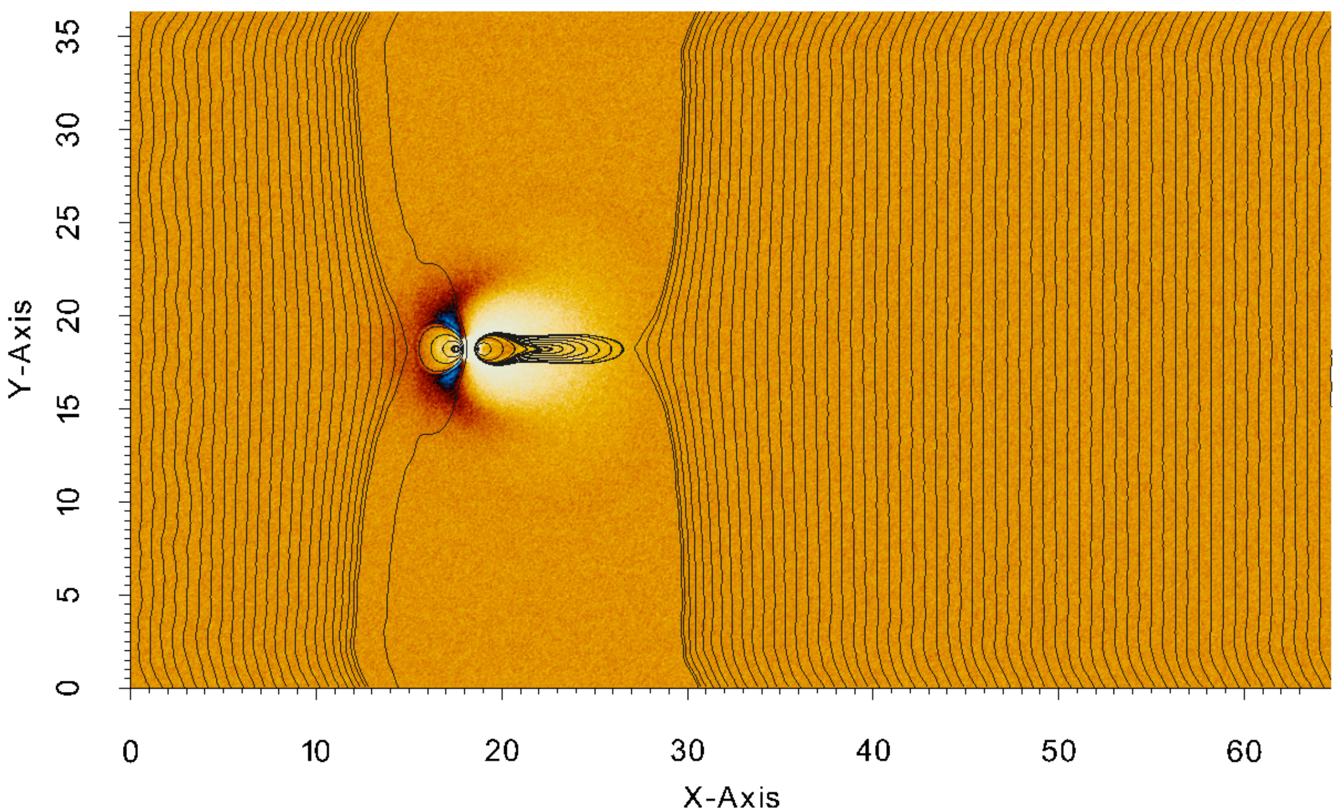

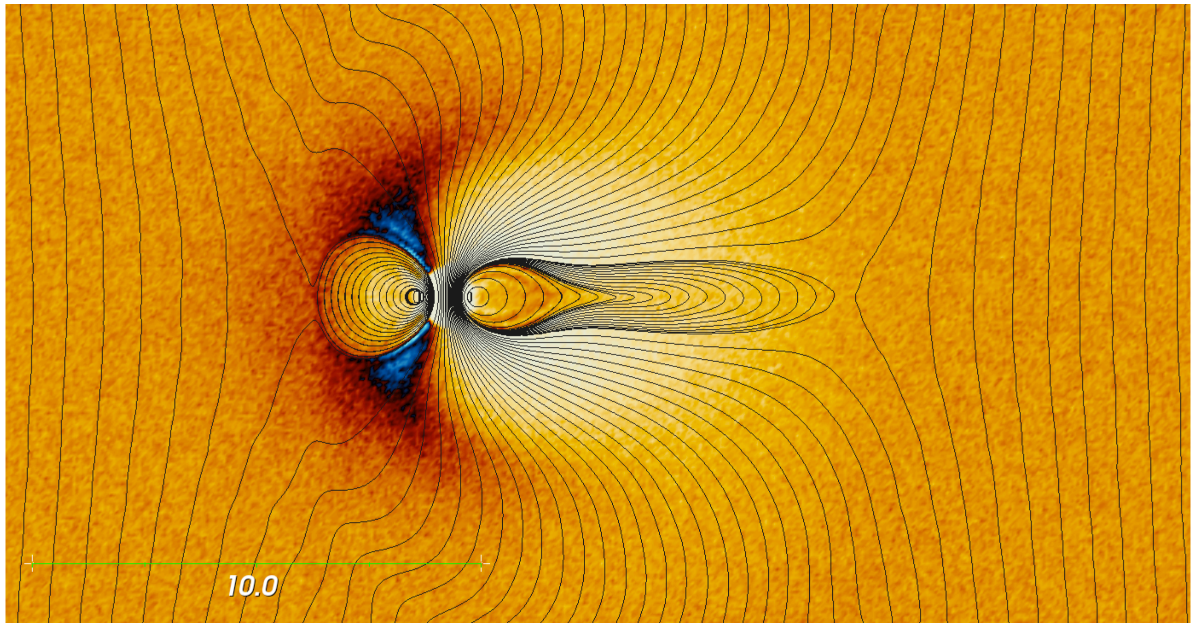

$$L_x = 64.768 d_i$$

$$L_y = 36.432 d_i$$

$$N = 1024 \times 576 = 589\,824$$

$$\Delta x = \Delta y = 0.06325 d_i$$

$$V_{sw}/c = 0.015$$

$$V_{th,e}/c = 0.05$$

$$V_{th,i}/c = 7.4 \times 10^{-3}$$

$$m_i/me = 250$$

$$M_A = 5$$

B. Equatorial plane

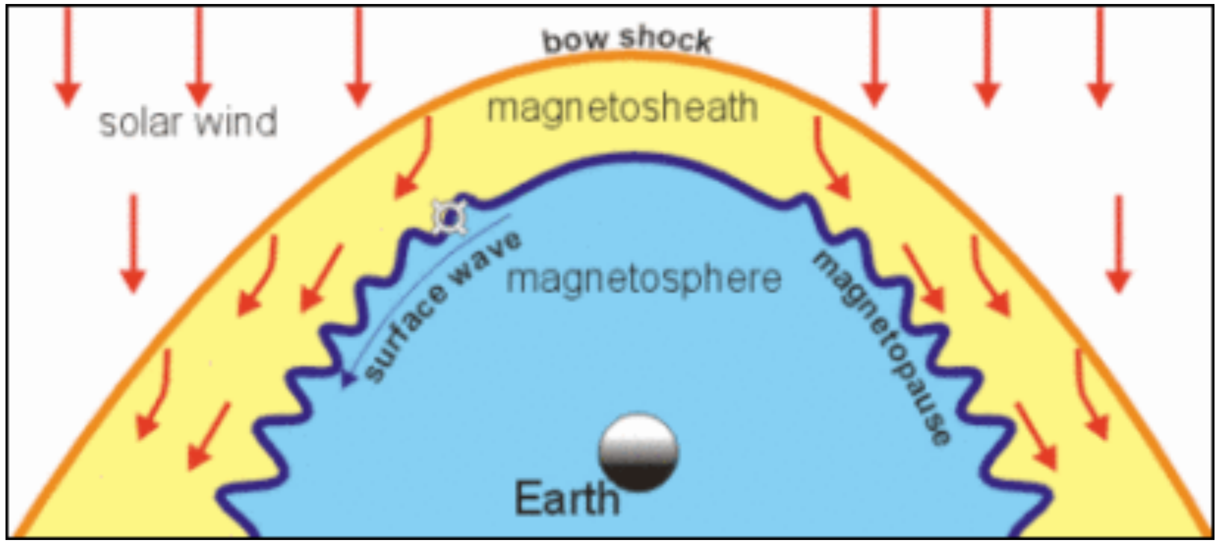

Diffusion effects at the boundary layer

[1] T. D. Phan and G. Paschmann, J. Geophys. Res., 101, 7801, (1996).

B. Equatorial plane

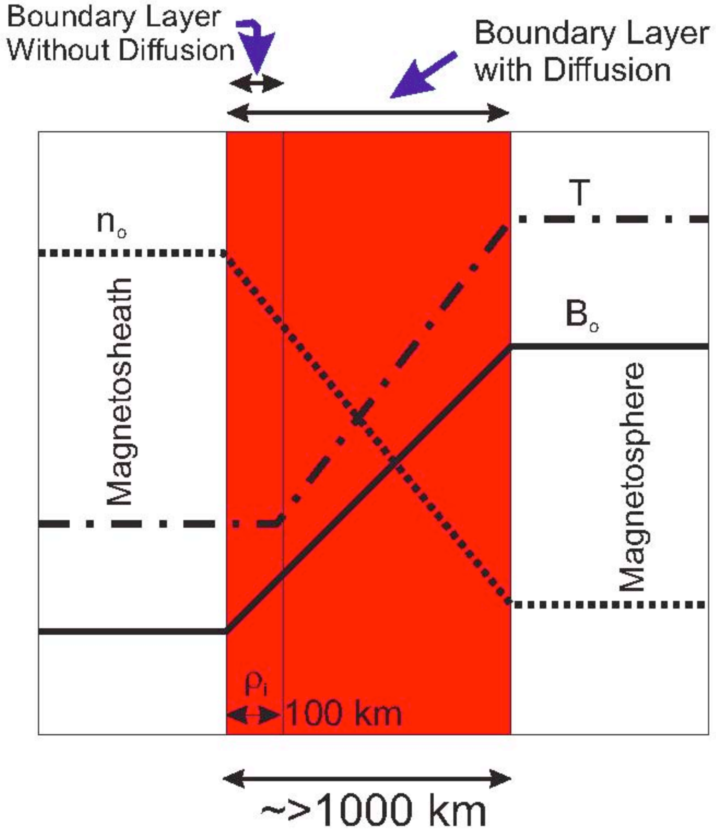

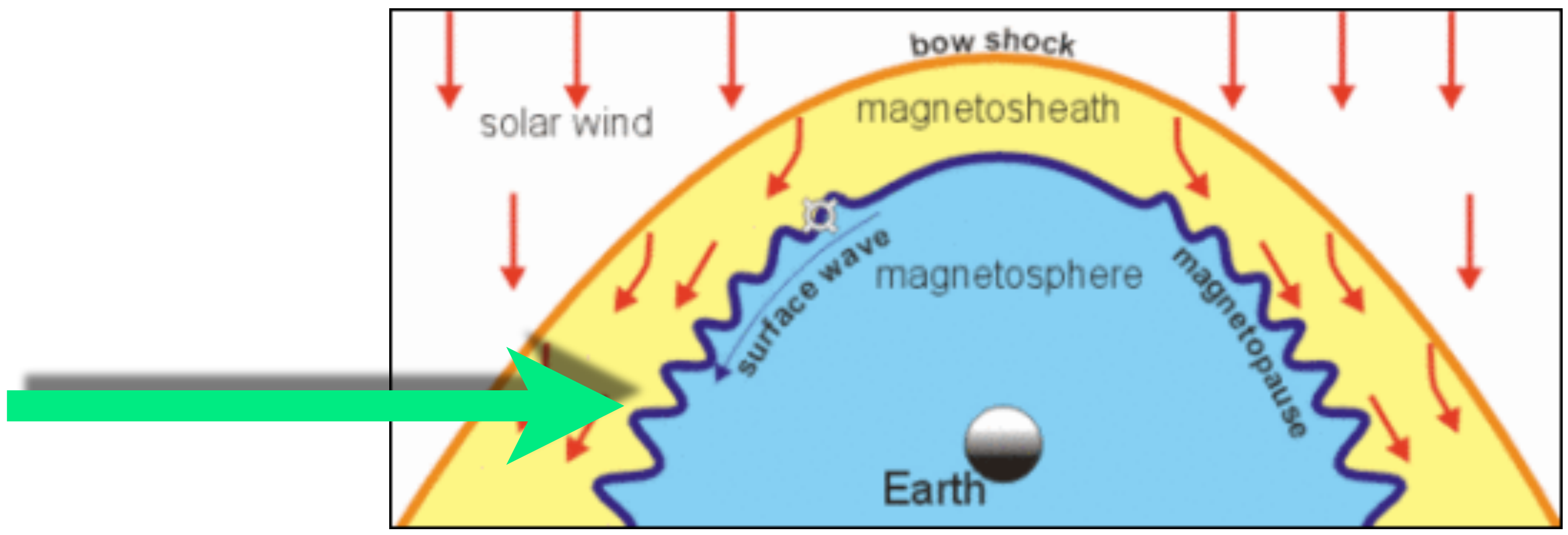

Diffusion effects at the boundary layer

[1] T. D. Phan and G. Paschmann, J. Geophys. Res., 101, 7801, (1996).

B. Equatorial plane

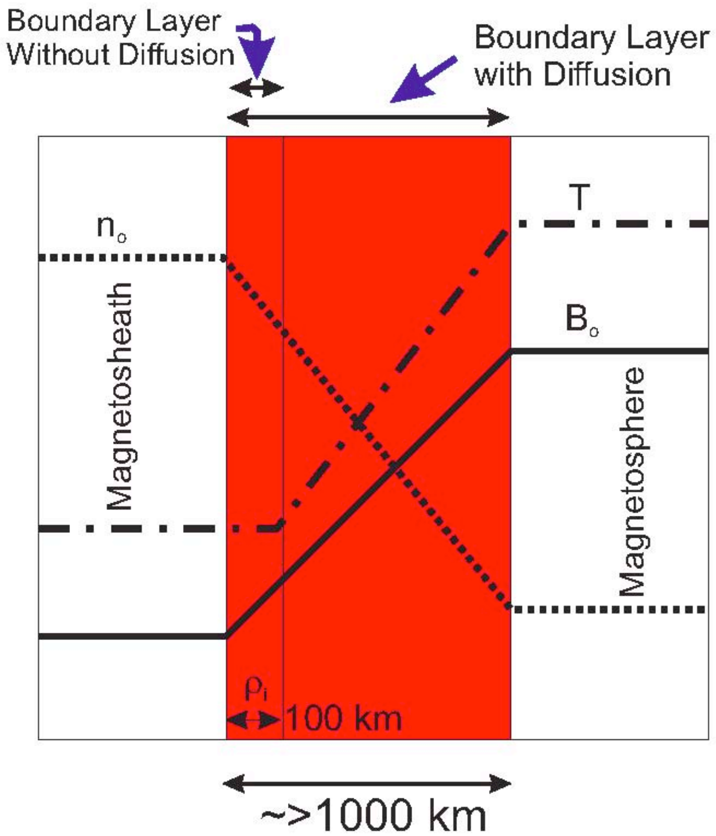

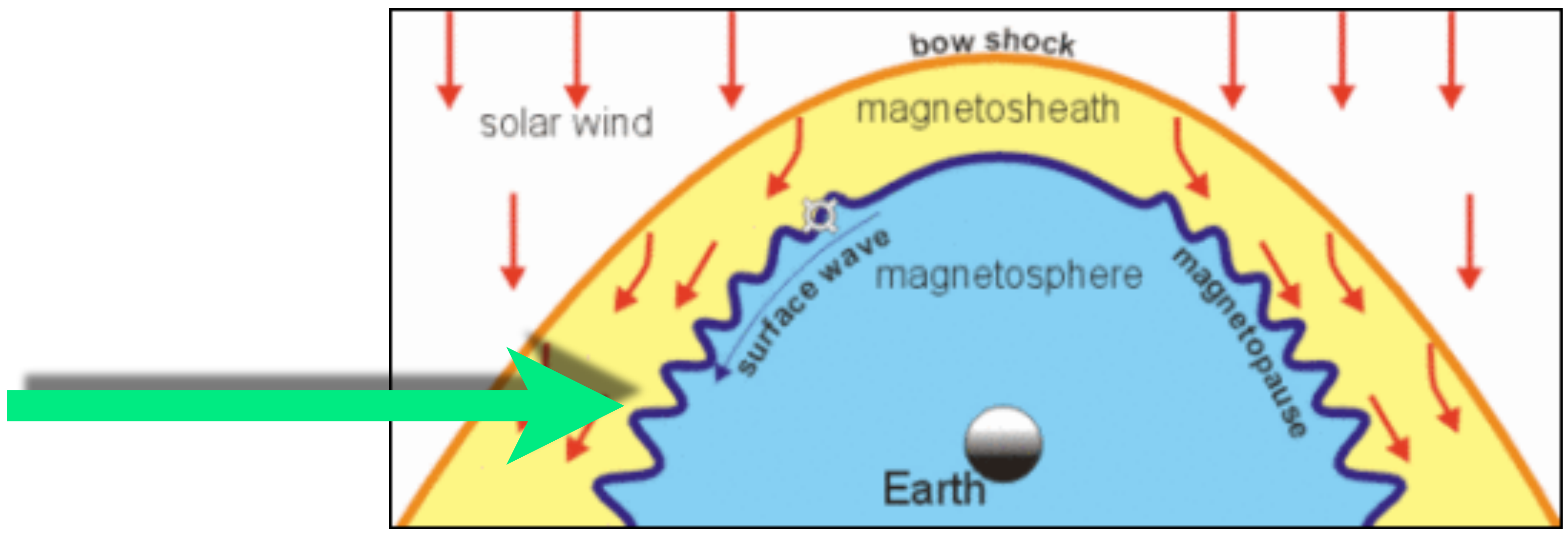

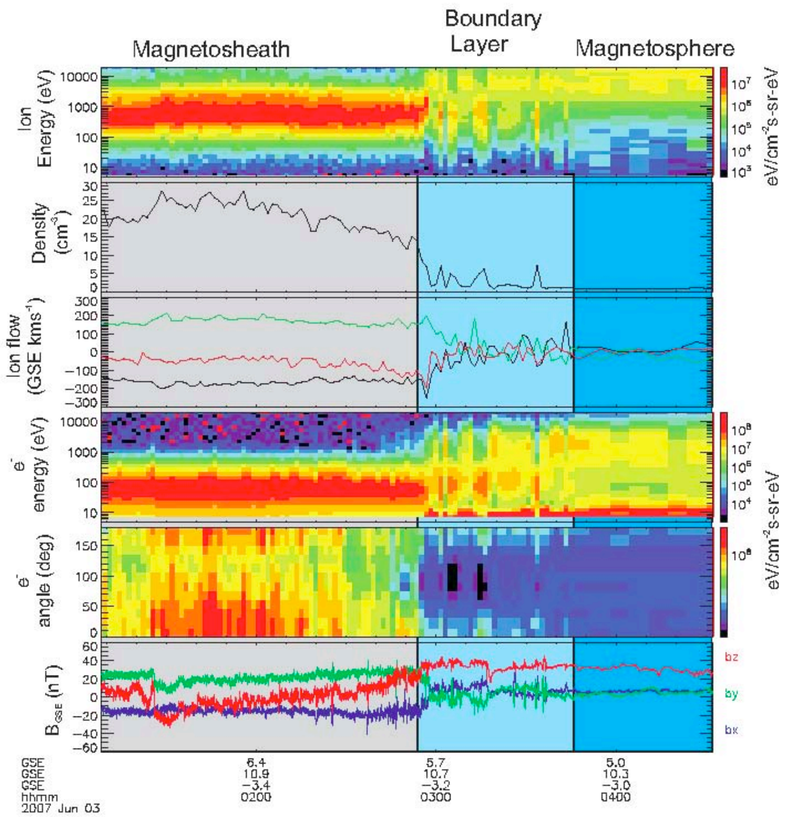

Diffusion effects at the boundary layer

[1] T. D. Phan and G. Paschmann, J. Geophys. Res., 101, 7801, (1996).

B. Equatorial plane

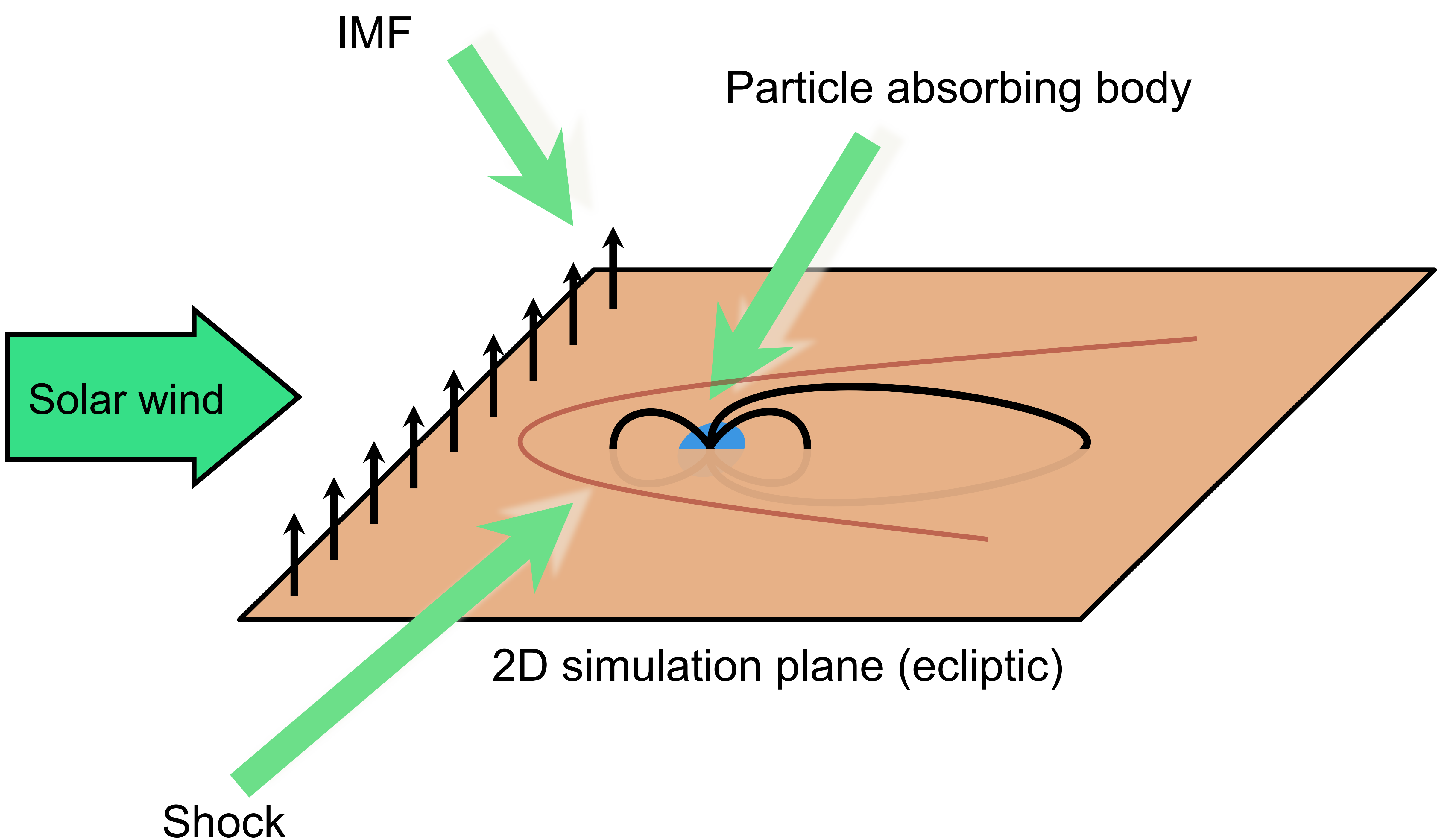

B. Equatorial plane: density

Simulation initialization 15 000 cycles,7 hours,
1024 processors, 1.7 Mcells, 88.5 Mparticles

B. Equatorial plane: density

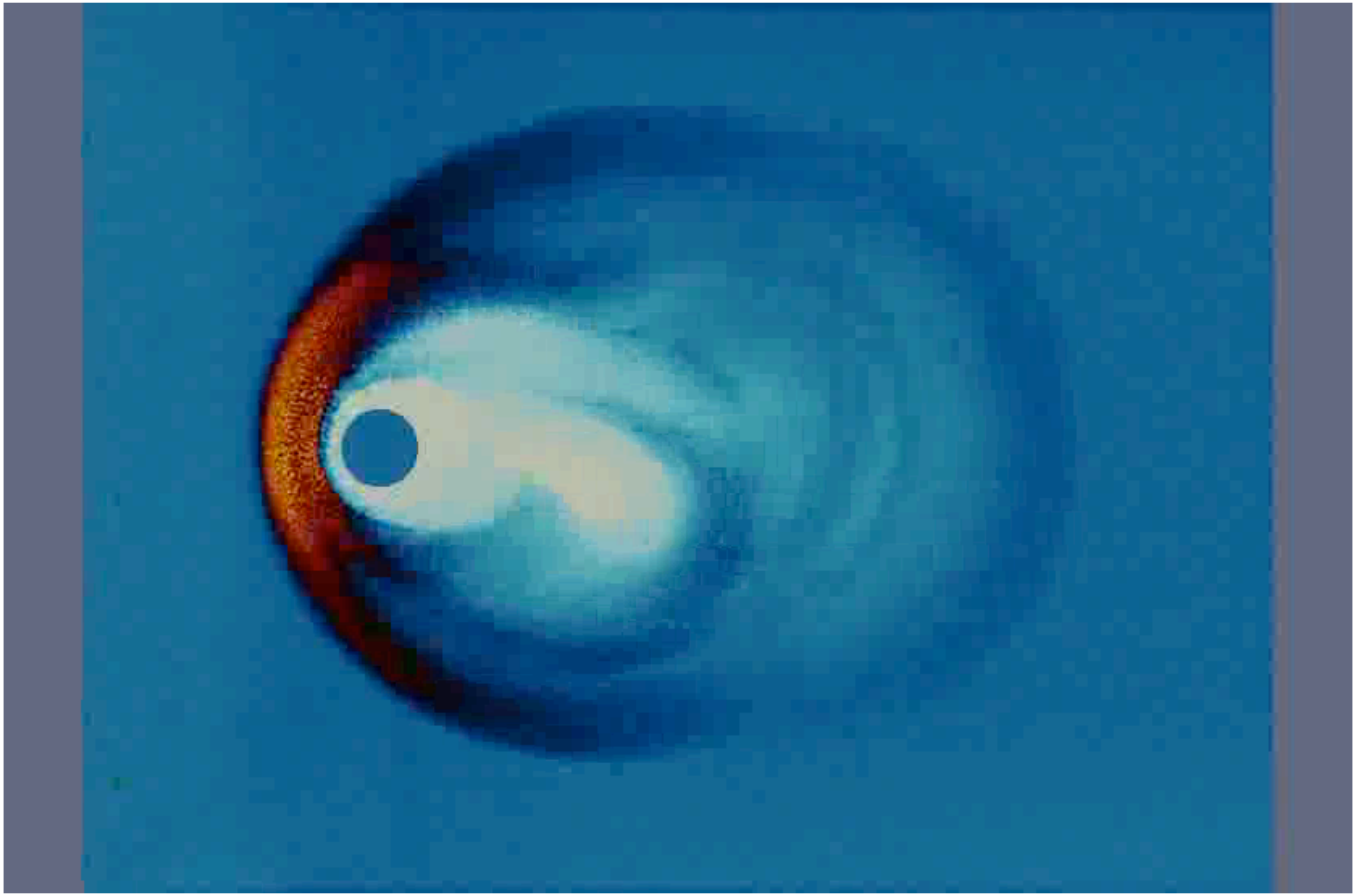

Simulation initialization 15 000 cycles,7 hours, 1024 processors, 1.7 Mcells, 88.5 Mparticles

B. simulation parametters

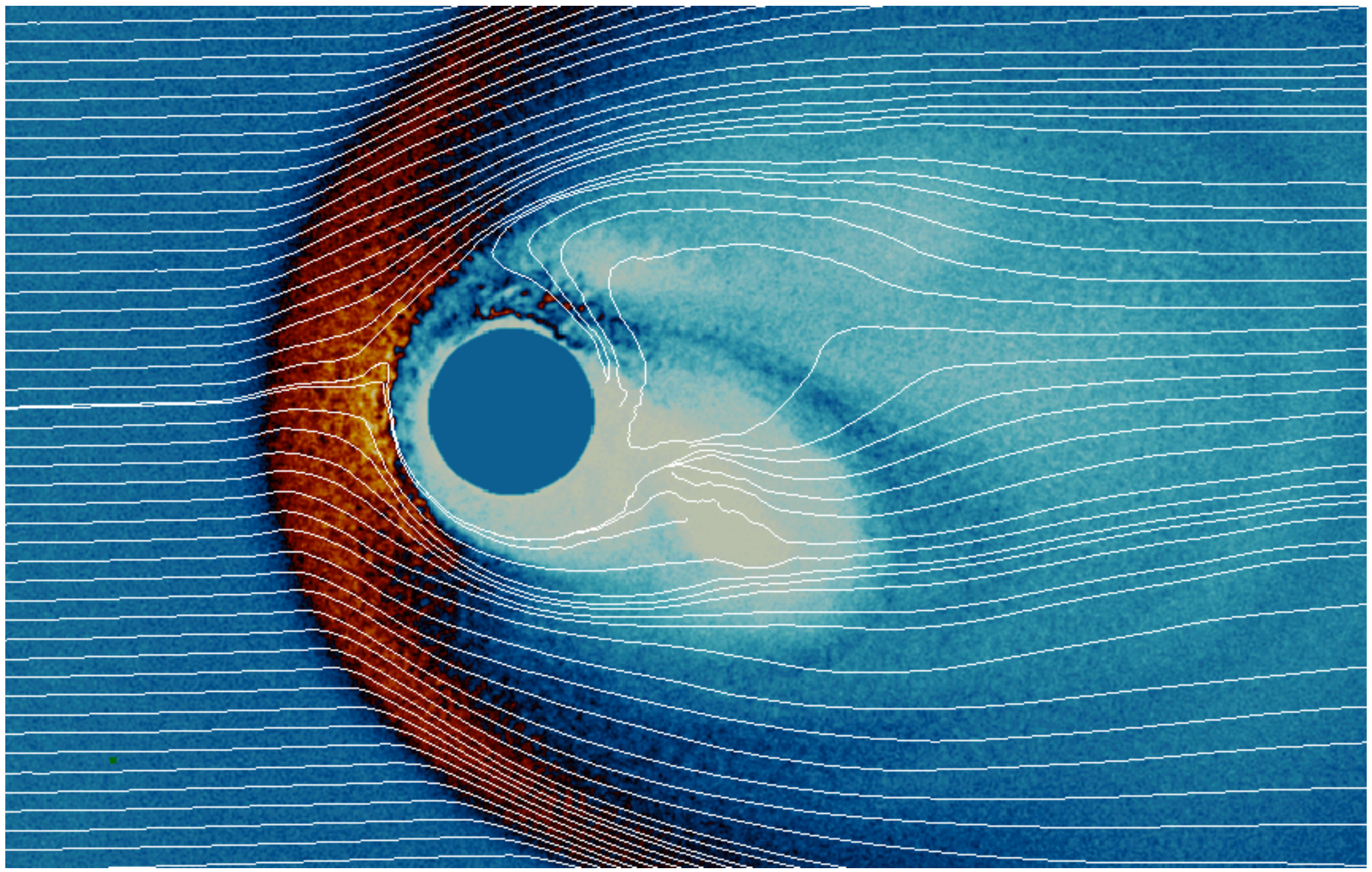

$$\Delta x = \Delta y = 0.04 d_i$$

$$V_{sw}/c = 0.003$$

$$V_{th,e}/c = 3.7 \times 10^{-3}$$

$$V_{th,i}/c = 2.35 \times 10^{-4}$$

$$m_i/me = 250$$

$$M_A = 5$$

KU LEUVEN

Comparison against an hybrid code

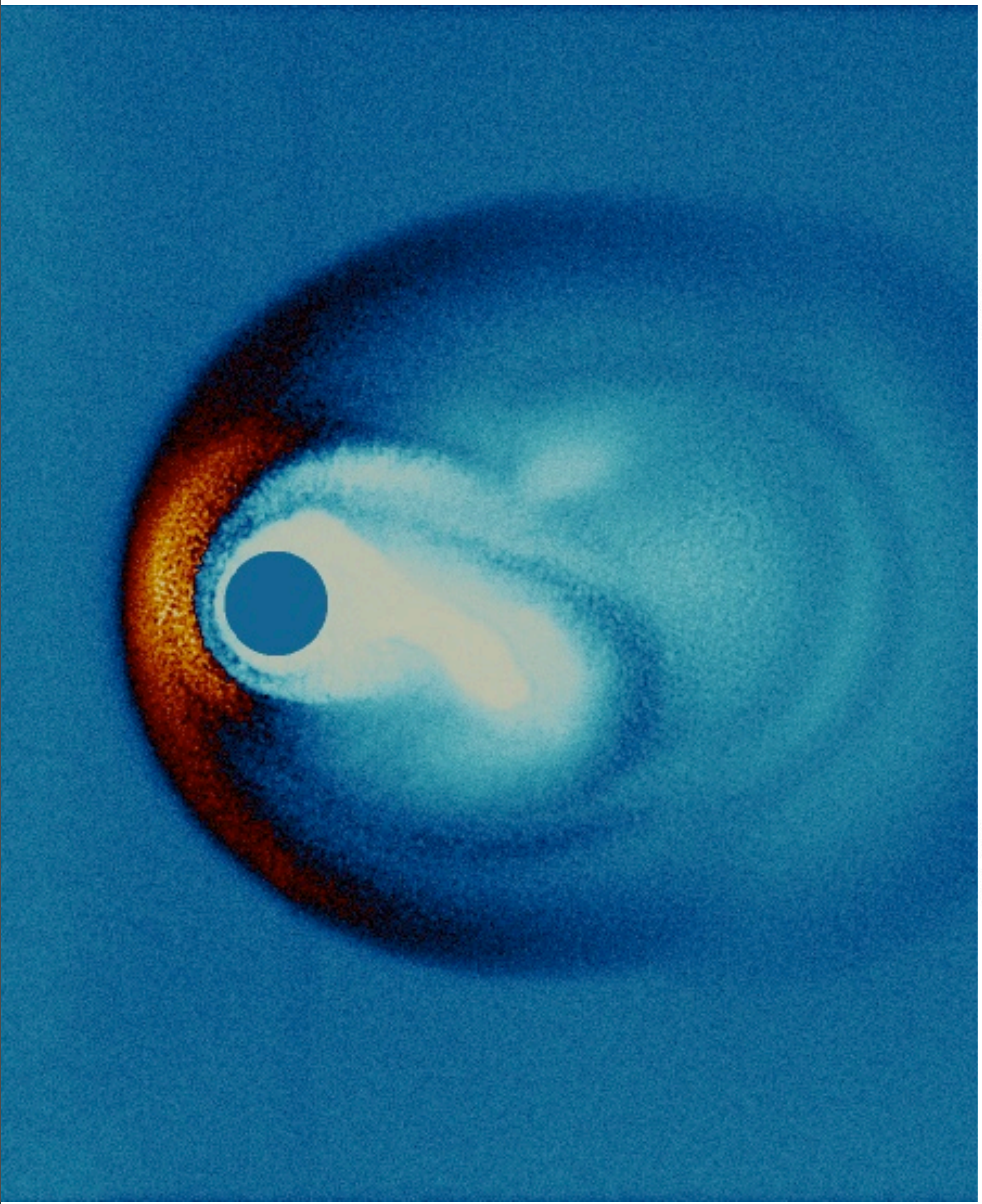

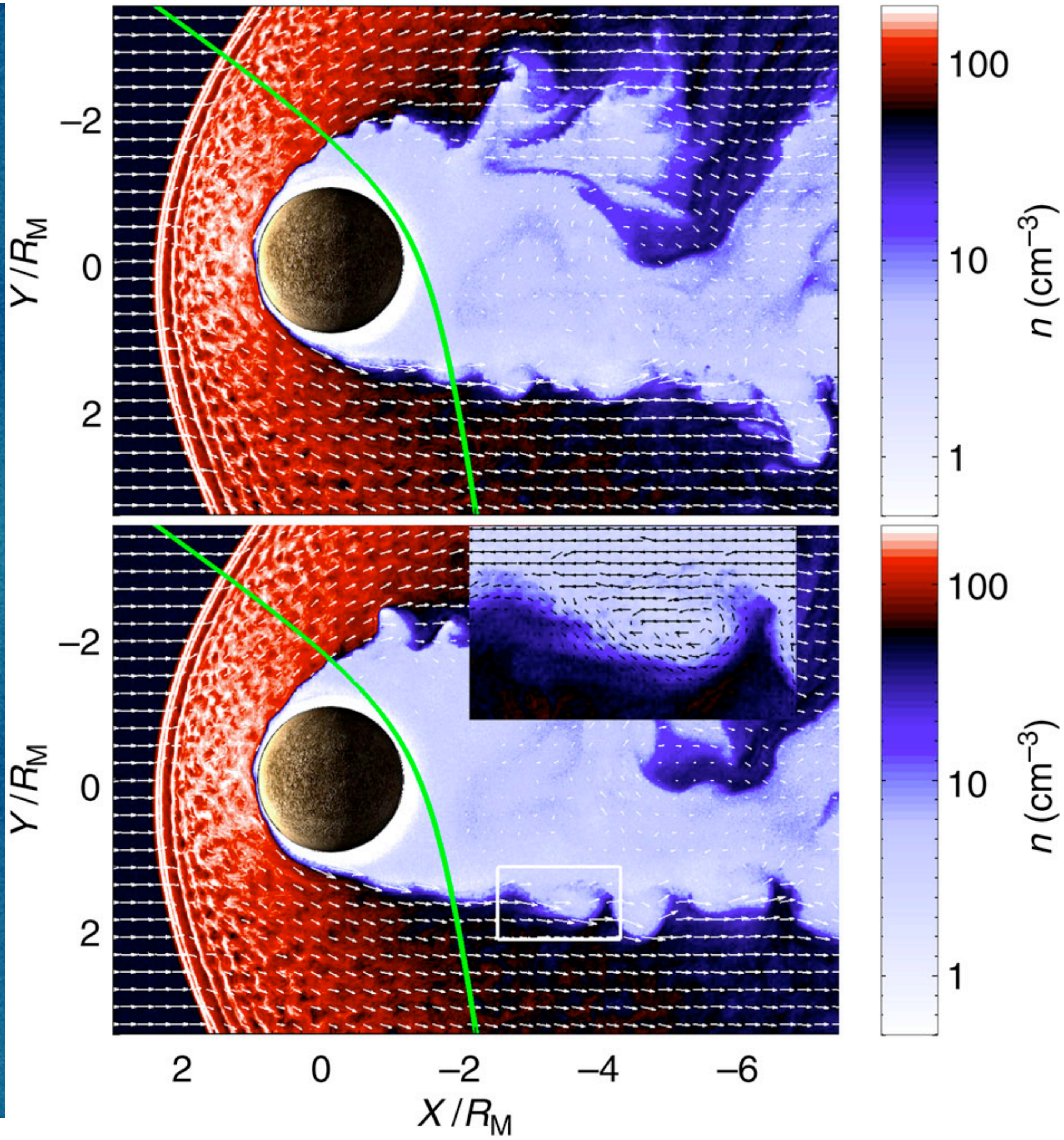

[1] J. Paral and R. Rankin, Nature Communications, 4 - 1645, April, 2013

B. Across the shock

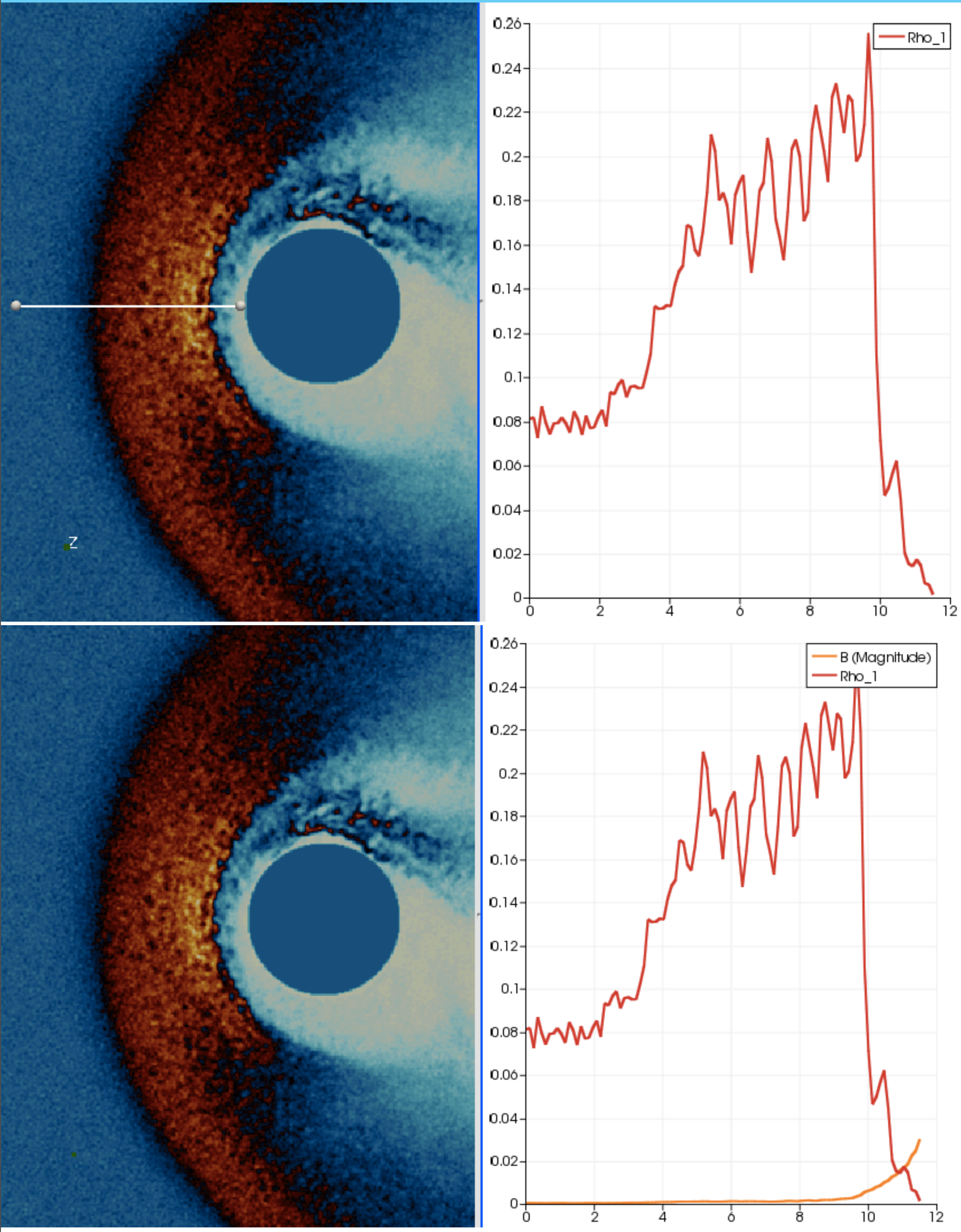

- 4 zones:
  - Interplanetary plasma
  - Magnetosheat
  - Diffusion zone
  - Magnetosphere
- Top: ion density
- Bottom: ion density and magnitude of the magnetic field

B. Dusk density profiles

- Density variation across the magnetosheat
- Sharp density drop across the magnetopause
- Instabilities in the plasma flow at the magnetopause

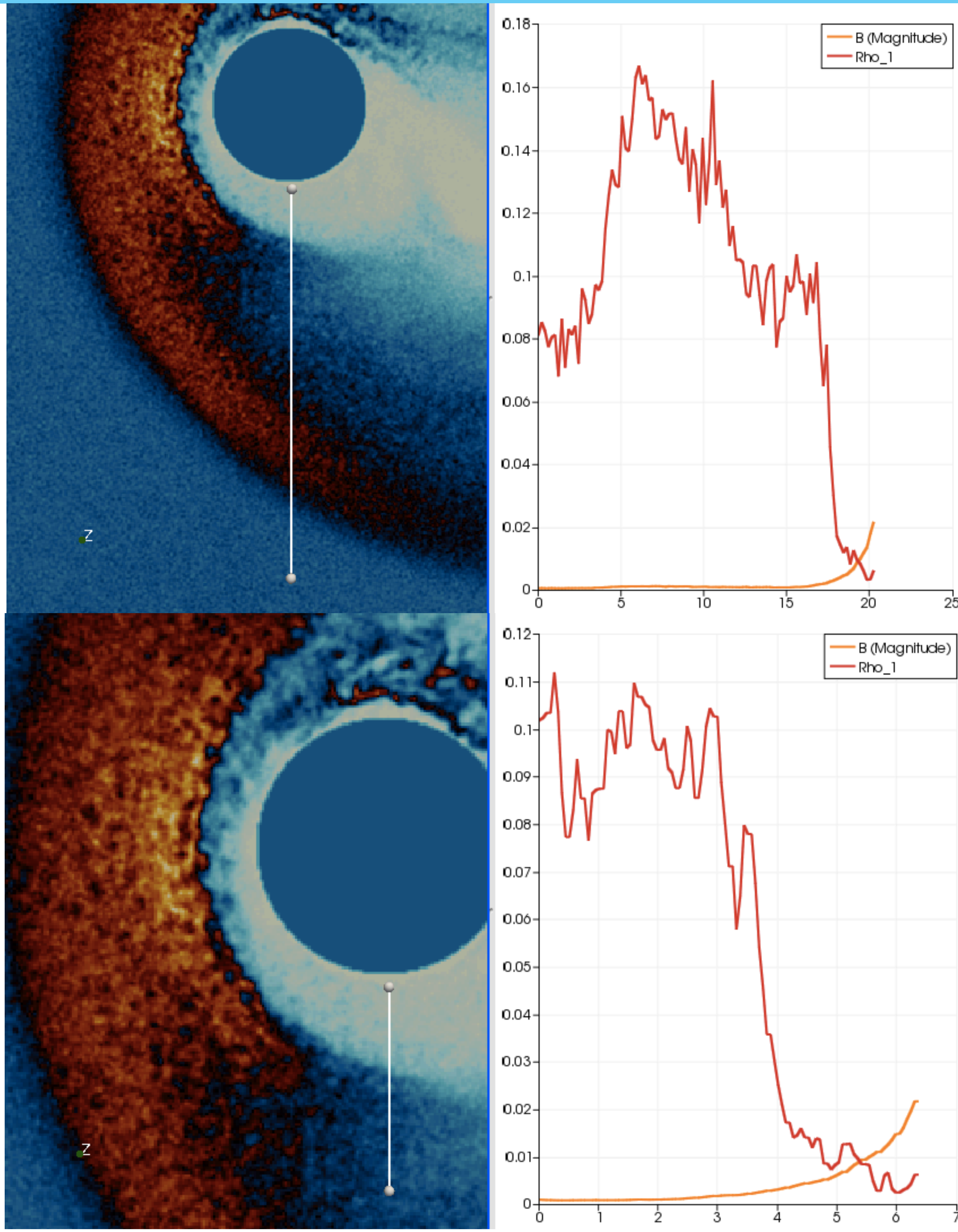

C. Future work

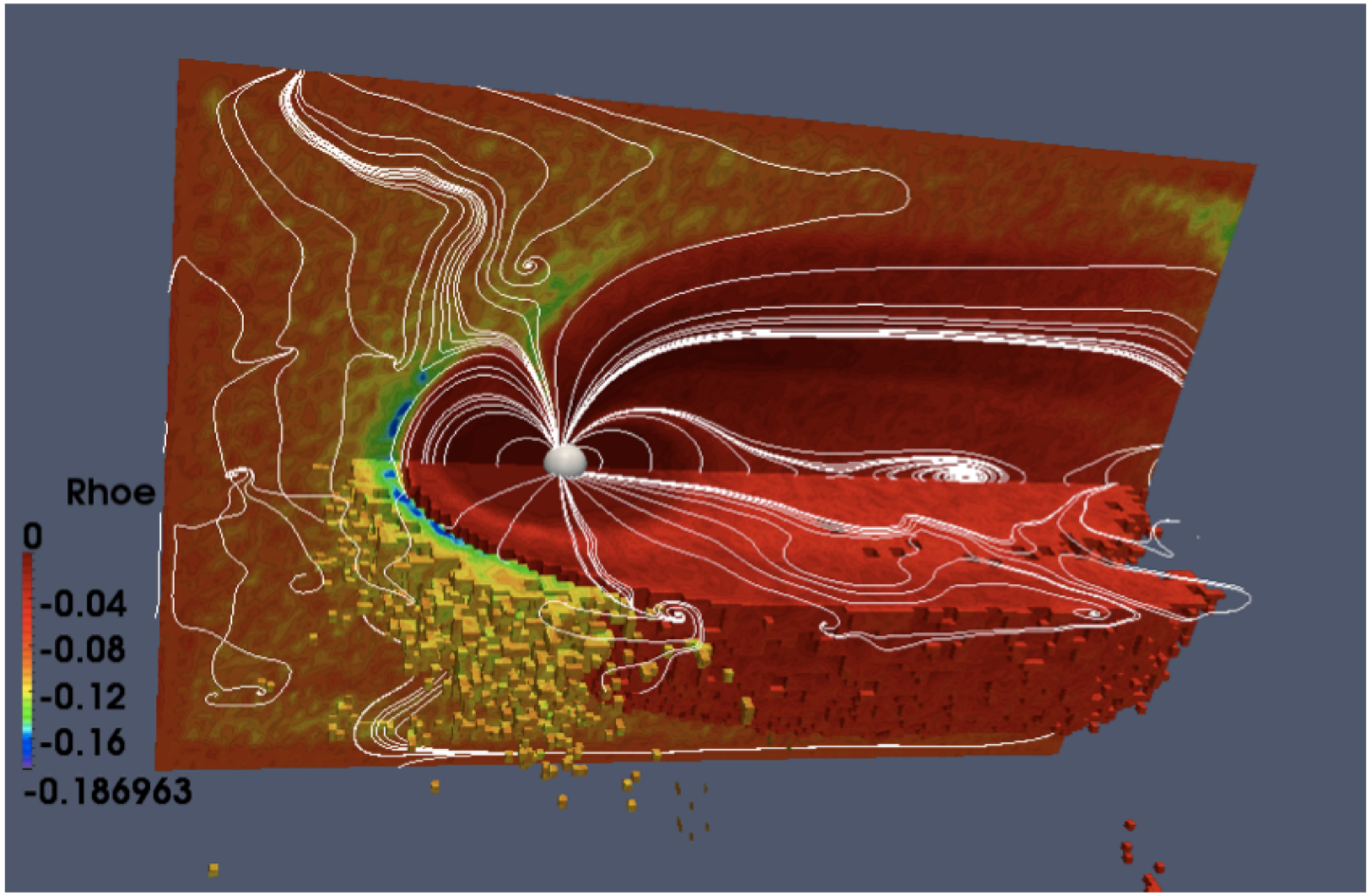

- Higher resolution
- Bigger planet
- Fully implicit
- Computations with up to 100 000 CPU cores
- Improvement of boundary conditions
- 3D system

Conclusions

- PiC methods are very sensitive to the thermal velocities imposed.
- Global simulations with electron-scale resolutions are yet computationally expensive.
- Boundary conditions are a major issue.
- We are pushing the code to the current computational limits.
- However we are currently performing simulations with parametters very close to those measured in-situ.

Towards the study of the Solar wind Effects on the Magnetosphere using Fully Kinetic Simulations

Jorge AMAYA[1], Jan DECA[1], Stefano Markidis[2], Andrei DIVIN[3], Bertrand Lembège[4], Giovanni LAPENTA[1]

[1]CPA, KULeuven, Belgium
[2]KTH Royal Institute of Technology, Sweden
[3]Institutet för rymdfysik, Uppsala Universitet, Sweden
[4]LATMOS, CNRS, France

KU LEUVEN

The iPiC3D code

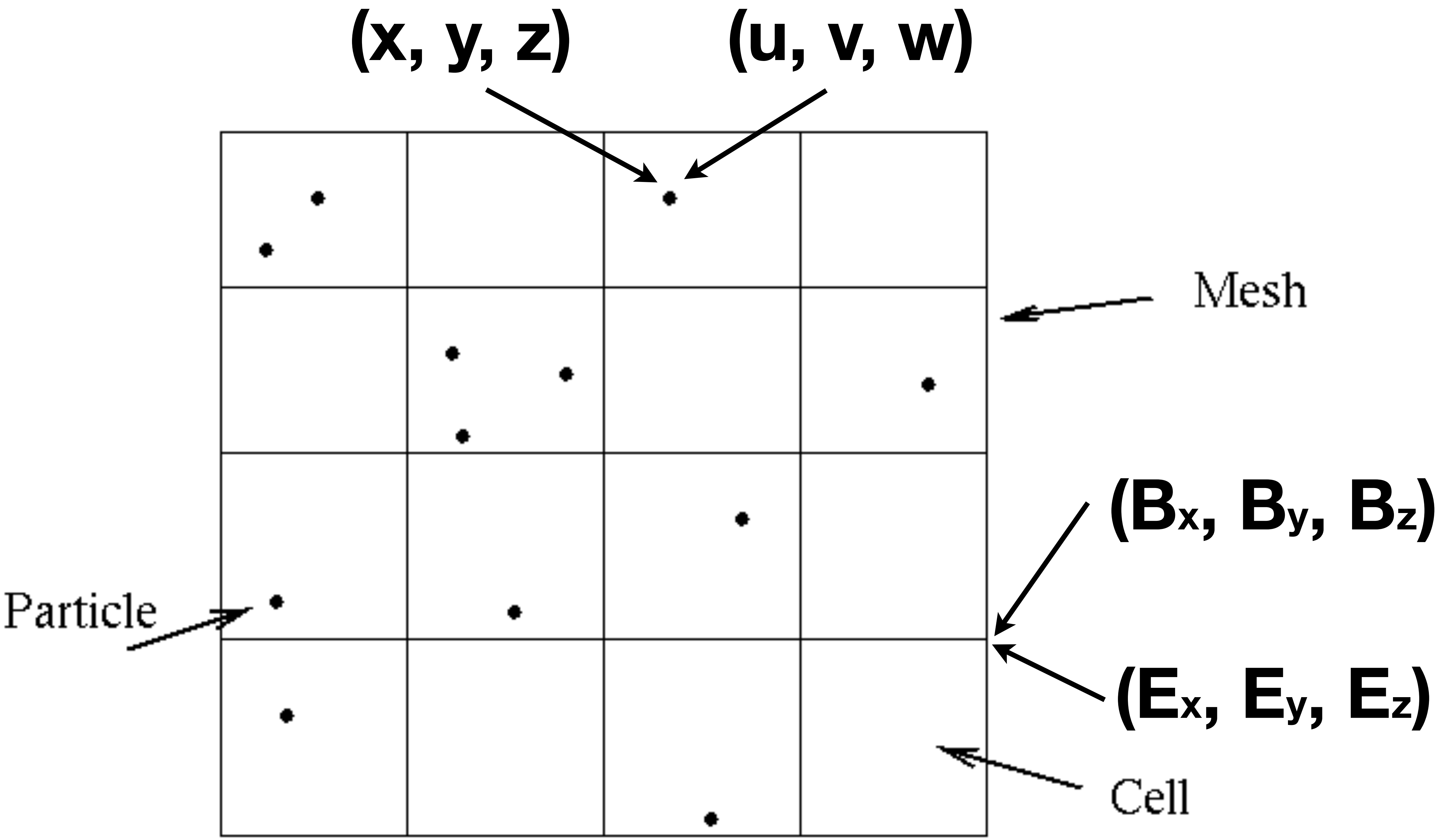

Moments

$$\rho_g^n = \frac{1}{V_g}\sum_p q_p W(\mathbf{x}_g - \mathbf{x}_p^n),$$

$$\mathbf{J}_g^n = \frac{1}{V_g}\sum_p q_p \mathbf{v}_p^n W(\mathbf{x}_g - \mathbf{x}_p^n),$$

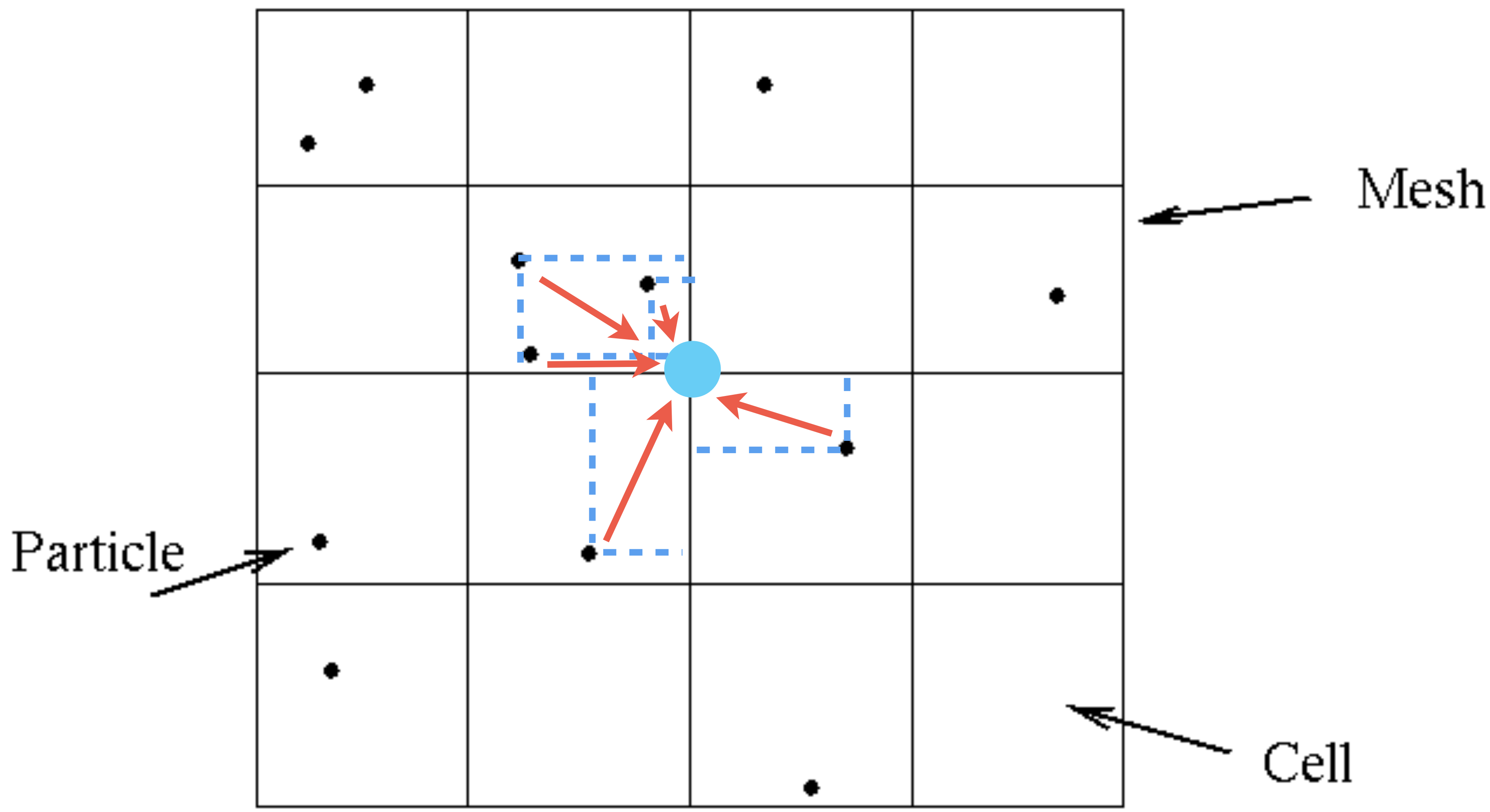

Field to particle interpolation

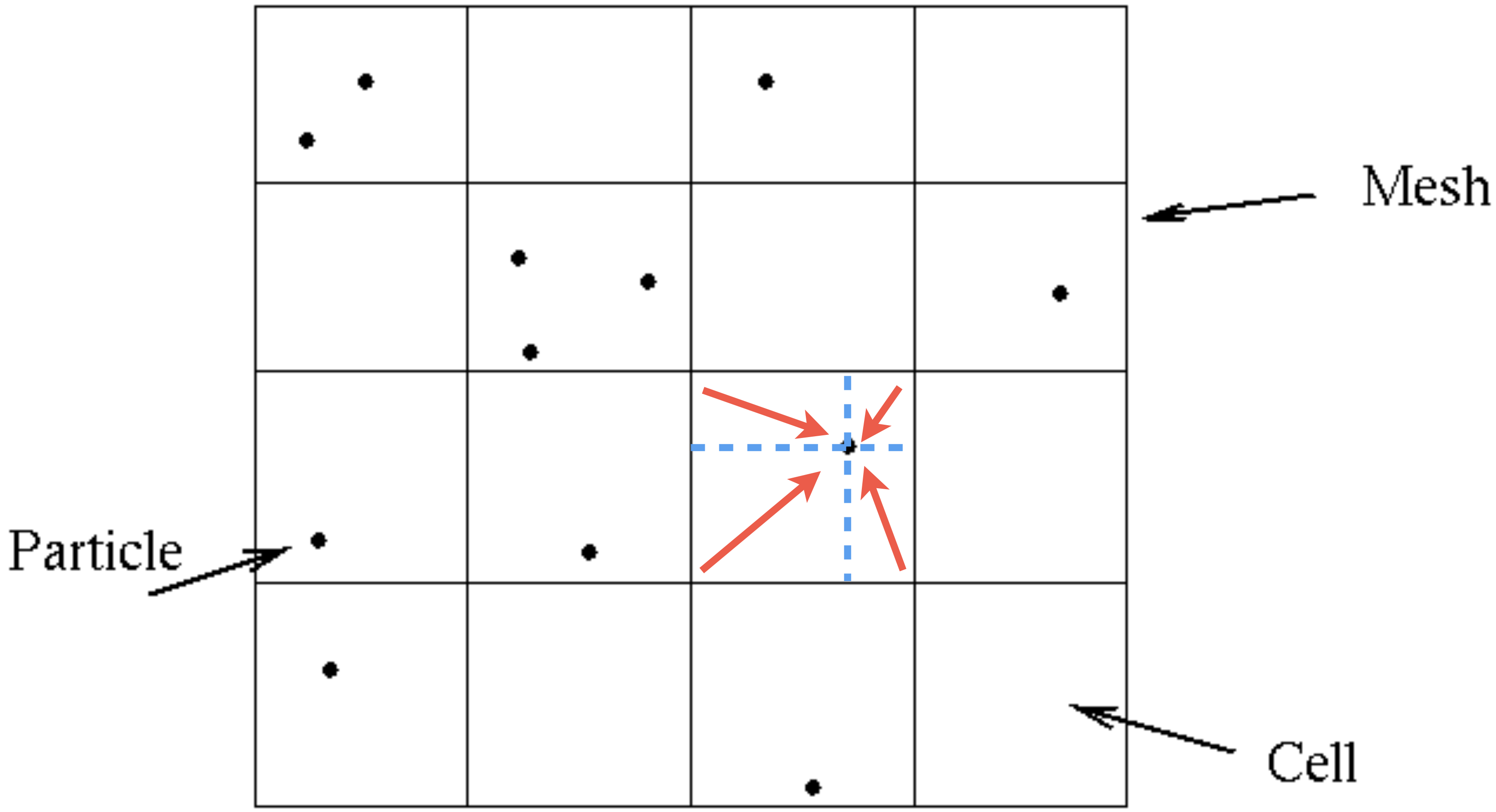

$$\mathbf{E}_p = \sum_g \mathbf{E}_g W(\mathbf{x}_g - \mathbf{x}_p),$$

$$\mathbf{B}_p = \sum_g \mathbf{B}_g W(\mathbf{x}_g - \mathbf{x}_g).$$

Implicit particle transport

$$\mathbf{x}_p^{n+1} = \mathbf{x}_p^n + \mathbf{v}_p^{n+1/2}\Delta t,$$

$$\mathbf{v}_p^{n+1} = \mathbf{v}_p^n + \frac{q_s \Delta t}{m_s}\left(\mathbf{E}_p^{n+\theta}(\mathbf{x}_p^{n+1/2}) + \mathbf{v}_p^{n+1/2} \times \mathbf{B}_p^n(\mathbf{x}_p^{n+1/2})\right)$$

$$\mathbf{v}_p^{n+1/2} = \widehat{\mathbf{v}}_p + \beta_s \widehat{\mathbf{E}}_p^{n+\theta}(\mathbf{x}_p^{n+1/2})$$

$$\widehat{\mathbf{v}}_p = \boldsymbol{\alpha}_p^n \cdot \mathbf{v}_p^n,$$

$$\beta_s = q_p \Delta t / 2m_p$$

$$\widehat{\mathbf{E}}_p^{n+\theta} = \boldsymbol{\alpha}_p^n \cdot \mathbf{E}_p^{n+\theta},$$

$$\boldsymbol{\alpha}_p^n = \frac{1}{1 + (\beta_s B_p^n)^2}\left(\boldsymbol{I} - \beta_s \boldsymbol{I} \times \mathbf{B}_p^n + \beta_s^2 \mathbf{B}_p^n \mathbf{B}_p^n\right),$$

Implicit Maxwell equations

$$\mathbf{B}_g^{n+1} - \mathbf{B}_g^n = -\Delta t \nabla \times \mathbf{E}_g^{n+\theta},$$

$$\mathbf{E}_g^{n+1} - \mathbf{E}_g^n = \frac{\Delta t}{\mu_0 \epsilon_0} \left(\nabla \times \mathbf{B}_g^{n+\theta} - \mu_0 \boxed{\mathbf{J}_g^{n+\frac{1}{2}}} \right),$$

$$\epsilon_0 \nabla \cdot \mathbf{E}_g^{n+\theta} = \boxed{\rho_g^{n+\theta}},$$

$$\nabla \cdot \mathbf{B}_g^{n+1} = 0.$$

Second order Maxwell

$$\mathbf{E}^{n+\theta} - (c\theta\Delta t)^2\nabla^2\mathbf{E}^{n+\theta} = \mathbf{E}^n + c^2\theta\Delta t\left(\nabla\times\mathbf{B}^n - \frac{\theta\Delta t}{\epsilon_0}\nabla\rho^{n+\theta} - \mu_0\mathbf{J}^{n+1/2}\right)$$

Taylor series expansion of the shape function:

$$S(\mathbf{x}-\mathbf{x}^{n+\theta}) = S(\mathbf{x}-\mathbf{x}^n) - (\theta\Delta t)\mathbf{v}^{n+\theta}\cdot\nabla S(\mathbf{x}-\mathbf{x}^n) + \cdots$$

Applying to the moments gives a linear interpolation:

$$\mathbf{J}^{n+1/2} \approx \widehat{\mathbf{J}}^n + \frac{\boldsymbol{\mu}^n}{\theta\Delta t}\cdot\mathbf{E}^{n+\theta},$$

$$\rho^{n+\theta} \approx \rho^n - \theta\Delta t\nabla\cdot\mathbf{J}^{n+1/2}$$

where

$$\left\{\begin{aligned}
\widehat{\mathbf{J}}^n(\mathbf{x}) &:= \sum_p q_p\widehat{\mathbf{v}}_p^n S(\mathbf{x}-\mathbf{x}_p^n) - \frac{\Delta t}{2}\nabla\cdot\sum_p q_p\widehat{\mathbf{v}}_p^n\widehat{\mathbf{v}}_p^n S(\mathbf{x}-\mathbf{x}_p^n),\\
\widehat{\rho}^n(\mathbf{x}) &:= \sum_p q_p S(\mathbf{x}-\mathbf{x}_p^n) - \theta\Delta t\nabla\cdot\widehat{\mathbf{J}}^n(\mathbf{x}).\\
\boldsymbol{\mu}^n &= \sum_s \frac{q_s\rho_s^n}{m_s}\frac{(\boldsymbol{I} - \beta_s\boldsymbol{I}\times\mathbf{B}^n + \beta_s^2\mathbf{B}^n\mathbf{B}^n)}{1+(\beta_s B^n)^2}.
\end{aligned}\right.$$

Final form for the E field equation

$$(c\theta\Delta t)^2\left[-\nabla^2\mathbf{E}^{n+\theta}-\nabla\nabla\cdot\left(\boldsymbol{\mu}^n\cdot\mathbf{E}^{n+\theta}\right)\right]+\boldsymbol{\epsilon}^n\cdot\mathbf{E}^{n+\theta}$$
$$=\mathbf{E}^n+(c\theta\Delta t)\left(\nabla\times\mathbf{B}^n-\mu_0\hat{\mathbf{J}}^n\right)-\frac{(c\theta\Delta t)^2}{\epsilon_0}\nabla\hat{\rho}^n,$$

$$\boldsymbol{\epsilon}^n=\mathbf{I}+\boldsymbol{\mu}^n$$

Stability condition:

$$v_{\mathrm{th},e}\Delta t/\Delta x<1.$$